Joint Fiber Nonlinearity Mitigation and Compensation for Digital Sub-Carrier Multiplexing System

Selvakumar Tharranetharan, *Member, IEEE*, Sunish Kumar Orappanpara Soman, *Senior Member, IEEE*, and Lutz Lampe, *Senior Member, IEEE*

***Abstract*—Fiber nonlinearity is the bottleneck of optical communication systems and is commonly addressed by applying various nonlinearity mitigation and compensation techniques. In general, nonlinearity mitigation techniques offer modest improvements with minimal computational complexity, while nonlinearity compensation techniques provide significant performance gains at the expense of higher computational complexity. This motivates us to propose a joint nonlinearity mitigation and compensation approach in which the nonlinear effects during signal propagation are reduced to compensate for the residual nonlinearity at a lower complexity. Specifically, in this paper, we study the combination of symbol rate optimization (SRO) and perturbation-based nonlinearity compensation (PB-NLC) for a pre-chromatic dispersion compensated (pre-CDC) transmission of polarization multiplexing, digital sub-carrier multiplexing, and wavelength division multiplexing (PM-DSCM-WDM) optical communication system. We highlight the interplay between SRO and PB-NLC and demonstrate that joint SRO and PB-NLC provides considerable performance gain, significant complexity reduction, and an additional degree of freedom to balance performance-complexity trade-offs when compared to applying only PB-NLC in a conventional PM-WDM system. We observe that the pre-CDC transmission manifests a unique property that enables the distribution of PB-NLC computational complexity between transmitter and receiver. Leveraging the distinctive property, we propose a split PB-NLC technique for the PM-DSCM-WDM system. This technique combines the benefits of both pre-PB-NLC and post-PB-NLC, resulting in a modest performance improvement while maintaining the same computational complexity as post-PB-NLC.**

***Index Terms*—Complexity-performance trade-off, cross-phase modulation (XPM), optical fiber communications, perturbation-based nonlinearity compensation (PB-NLC), split technique, sub-carrier multiplexing, symbol rate optimization (SRO).**

Manuscript received 9 July 2024; accepted 13 July 2024. Date of publication 16 July 2024; date of current version 29 July 2024. This work was supported in part by the Huawei Tech., Canada, in part by the Digital Research Alliance of Canada through computational resources and services (www.alliancecan.ca), and in part by the Advanced Research Computing at the University of British Columbia. *(Corresponding author: Lutz Lampe.)*

Selvakumar Tharranetharan and Lutz Lampe are with the Department of Electrical and Computer Engineering, The University of British Columbia, Vancouver, BC V6T 1Z4, Canada (e-mail: tharrane@ece.ubc.ca; lampe@ece.ubc.ca).

Sunish Kumar Orappanpara Soman was with the Department of Electrical and Computer Engineering, The University of British Columbia, Vancouver, BC V6T 1Z4, Canada. He is now with the Advanced Wireless Technologies Lab, Quantum Information and Communications Research, Ulster University, BT15 1ED Belfast, U.K. (e-mail: S.Orappanpara_Soman@ulster.ac.uk).

Digital Object Identifier 10.1109/JPHOT.2024.3429381

I. Introduction

THE increasing capacity demands due to the exponential growth in global information exchange necessitates optical fiber communication systems to continuously improve [1]. This has been accomplished over the past decades with the introduction of new techniques such as wavelength division multiplexing (WDM) [2], polarization multiplexing (PM) [3], coherent detection [4], and advanced modulations [5]. Furthermore, limitations of optical devices such as oscillators and filters in handling higher bandwidth signals have prompted the development of digital sub-carrier multiplexing (DSCM) [6]. DSCM systems process multiple parallel signals in the radio frequency domain and subsequently multiplex them into a single-wavelength signal in the optical domain. Thus, DSCM systems overcome the limitations of optical devices by leveraging advanced radio frequency counterparts [7]. Moreover, DSCM seamlessly integrates into existing WDM systems to increase the overall data-rate performance of optical fiber communication systems.

Changes in the refractive index of optical fibers proportional to the transmission power give rise to nonlinear distortions in signals known as the Kerr nonlinear effects [8]. The Kerr nonlinear effects fundamentally limit the capacity of the optical fiber communication medium. In WDM systems, the Kerr nonlinearity introduces self-phase modulation (SPM), cross-phase modulation (XPM), and four-wave mixing (FWM) [8]. SPM occurs due to the neighboring pulses' interaction within a single channel. In contrast, XPM and FWM arise due to the interaction of pulses between WDM channels, and their behavior is influenced by the channel spacing between these channels.

In DSCM systems, digital sub-carriers carrying different signals occupy distinct frequency bands within a WDM channel in the optical domain. Hence, the closely spaced digital sub-carriers experience SPM within a sub-carrier as well as inter-sub-carrier XPM (iXPM) and inter-sub-carrier FWM (iFWM), in addition to the inter-channel XPM and FWM effects observed in conventional WDM systems.[1] The impact of these nonlinear

[1] Some literature, e.g. [9], [10], categorize intra-channel nonlinear interactions into three types: SPM, intra-channel cross-phase modulation (IXPM), and intra-channel four-wave mixing (IFWM). In this work, we use SPM to account for all of these effects within a DSCM subcarrier, as in e.g, [11], [12]. Furthermore, the abbreviations iXPM and iFWM for cross sub-carrier nonlinear effects are used to avoid confusion with the abbreviations IXPM and IFWM used in the above-mentioned literature.

effects varies with the sub-carrier symbol rate [12]. At a higher symbol rate, the SPM effects dominate the nonlinearity of the DSCM system. As the sub-carrier symbol rate decreases, and accordingly the number of sub-carriers increases, iXPM and eventually iFWM effects become significant. But while iXPM diminishes after reaching a certain number of sub-carriers, iFWM effects continue to grow [12]. These differing trends among the nonlinear effects lead to a pattern where the aggregate nonlinear distortion initially decreases and then increases again with decreasing sub-carrier symbol rate. Consequently, there is an optimal sub-carrier symbol rate that minimizes the overall impact of nonlinear impairments in the DSCM systems [13].

Symbol rate optimization (SRO) in DSCM systems is an example of *nonlinearity mitigation.* Nonlinearity mitigation techniques aim to modify signal properties with the goal of improving tolerance against fiber nonlinearity during signal propagation. Other examples include pulse shaping [14] and dispersion management [15]. Alternatively, the detrimental effects of fiber nonlinearity can be addressed by *nonlinearity compensation*. Nonlinearity compensation techniques focus on estimating the induced nonlinear distortions and compensating them either at the transmitter through pre-compensation or at the receiver through post-compensation. Examples of nonlinearity compensation techniques include digital backpropagation (DBP) [16], Volterra series-based nonlinear equalizers [17], perturbation-based nonlinearity compensation (PB-NLC) [18], [19], [20], [21], phase-conjugate twin waves [22], and adaptive equalizers [11], [23], [24]. Generally, nonlinearity compensation provides significant performance gains with a corresponding increase in the computational complexity [16], [17], [18]. Nonlinearity mitigation offers comparatively moderate performance gains but with lower or negligible computational complexity [12], [14].

Most of the existing literature considers nonlinearity compensation and mitigation techniques independently, e.g., [11], [12], [13], [14], [16], [17], [18], [19], [20], [21], [22], [23], [24], [25]. However, combining these two approaches holds the promise of an overall improved performance-complexity trade-off. This is because nonlinearity compensation only needs to deal with the residual nonlinear effects when applying mitigation techniques. An example of this is given in [15], where the joint use of chromatic dispersion management and PB-NLC for SPM compensation is considered. The chromatic dispersion causes pulse broadening during fiber propagation, and these broadened pulses' interaction results in nonlinear effects [26]. Since PB-NLC estimates nonlinear effects considering these pulse interactions [19], reducing the pulse interactions by chromatic dispersion compensation (CDC) at the transmitter, i.e., pre-CDC, simplifies the PB-NLC. In [27], [28], [29], SRO for DSCM and DBP for the full band of the WDM channel of interest (COI) are combined. The quantitative performance results indicate that the optimal symbol rate for full-band DBP remains the same as when using linear compensation without DBP. This is because DBP addresses SPM, iXPM, and iFWM effects evenly, while linear compensation does not account for any nonlinear effects. Hence, the study [27] does not clearly show the interplay when combining nonlinearity mitigation and compensation techniques. Further, the primary challenge associated with DBP lies in its substantial computational complexity [11].

In this paper, we build on and extend the work from [15] and [27] in several ways. We consider polarization multiplexed DSCM-WDM transmission (PM-DSCM-WDM) as a preferred solution for high data-rate optical fiber communication and investigate the trade-offs afforded by joint fiber nonlinearity mitigation and compensation. For the former, we apply pre-CDC (as in [15]) and SRO (as in [27], [28], [29]). For the latter, different from [27], [28], [29], we focus on PB-NLC. This is because PB-NLC offers the capability to address a limited range of nonlinear effects while allowing for complexity adjustments [30]. Different from [15], we utilize PB-NLC to compensate for both SPM and XPM effects, e.g., [18], [20], [30], [31], [32] and [21], [33], respectively. In particular, we incorporate SPM and iXPM compensation at the receiver, which we refer to as post-PB-NLC, while considering SRO. Using perturbation analysis, we find that the pre-CDC permits an impressive reduction in SPM compensation complexity while its impact on iXPM complexity is minimal. However, we show that pre-CDC transmission results in a unique characteristic of iXPM distortions that enables us to distribute iXPM compensation between transmitter and receiver without any additional computational complexity. Leveraging this property of iXPM, we propose a split PB-NLC technique for PM-DSCM-WDM systems that performs nonlinearity compensation in two distinct phases: one for compensating iXPM effects arising from the first half of the propagation at the transmitter, and another for addressing full SPM effects and iXPM effects arising from the second half of the propagation at the receiver. The split PB-NLC technique reduces the nonlinearity compensation complexity at the receiver by sharing the iXPM compensation complexity between transmitter and receiver. Additionally, this technique provides a more accurate first-order perturbation approximation and combines the benefits of both pre-PB-NLC and post-PB-NLC.

Our numerical performance results demonstrate the interplay between SRO and PB-NLC when employed in the PM-DSCM-WDM optical communication system. In particular, we show that the optimal symbol rate depends on which (SPM, iXPM, and/or iFWM) and to what extent (the number of adjacent DSCM sub-carriers considered for iXPM compensation) nonlinear effects are compensated. Furthermore, the proposed joint SRO and post-PB-NLC realizes a favorable performance-complexity trade-off, such as a 0.25 dB improvement in Q^2-factor at a tenfold reduction in complexity, compared to a conventional PM-WDM system with post-PB-NLC. Joint SRO and post-PB-NLC also provides an additional degree of freedom in selecting the number of adjacent DSCM sub-carriers considered in the PB-NLC to facilitate reaching a desired complexity-performance trade-off. In this context, the proposed split PB-NLC technique evenly divides the computational complexity of PB-NLC between transmitter and receiver and delivers a modest performance improvement.

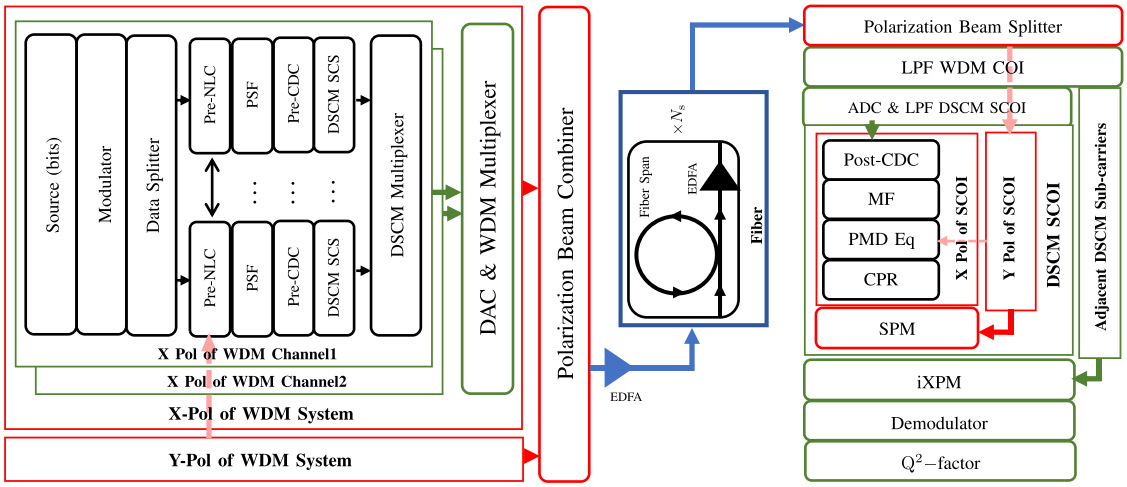

Fig. 1. The system model for the PM-DSCM-WDM system. PSF: pulse shaping filter, SCS: sub-carrier selection, DAC: digital-to-analog converter, EDFA: erbium-doped fiber amplifier, N_s: number of spans, LPF: low pass filter, SCOI: sub-carrier of interest, MF: matched filter, PMD Eq: polarization mode dispersion equalizer, CPR: carrier phase recovery.

The main contributions of this paper can be summarized as follows:

- We explore joint nonlinearity mitigation and compensation within the PM-DSCM-WDM system, incorporating SRO, pre-CDC transmission, and PB-NLC. The joint nonlinearity mitigation and compensation provides improved performance-complexity trade-offs while facilitating adaptability to diverse performance and/or complexity requirements demanded by real-world applications in optical communication systems.
- We derive the first-order iXPM perturbation coefficients of post-PB-NLC at the receiver for pre-CDC transmission in the PM-DSCM-WDM system, marking a novel contribution as no prior work has explored these characteristics of iXPM for pre-CDC transmission.
- Leveraging a unique property of iXPM in the context of pre-CDC transmission, we propose a novel split PB-NLC technique that offers multiple advantages over post-PB-NLC. A comprehensive insight and derivation of this split PB-NLC are presented.
- We use numerical simulations to illustrate that the optimal symbol rate for the joint nonlinearity mitigation and compensation approach hinges on the nonlinear effects compensated by PB-NLC and the degree to which these effects are compensated. Our study underscores the benefits of considering the nonlinear compensation's impact on the optimal symbol rate selection, a factor often overlooked in existing literature.
- In addition, we present valuable insights into the characteristics of PB-NLC within the PM-DSCM-WDM system, its flexibility in achieving desired performance-complexity trade-offs, the impact of complexity reduction techniques, and the advantages offered by the novel split PB-NLC technique.

The remainder of the paper is organized as follows. Section II describes the considered PM-DSCM-WDM system. Sections III and IV introduce the combined SRO and post-PB-NLC and the split PB-NLC technique, respectively. The characteristics, performance, and complexity of the joint nonlinearity mitigation and compensation techniques are presented and discussed in Section V. Finally, Section VI concludes the paper and highlights the key findings. The Appendices provide comprehensive mathematical derivations and valuable insights into the novel concepts explored in this paper.

A. Notation

Throughout this paper, bold letters are used to represent two-element single-column vectors containing the x- and y-polarizations components, as in $\boldsymbol{u} = u = [u \text{ of } \mathrm{x}-\mathrm{pol}, u \text{ of } \mathrm{y}-\mathrm{pol}]^{\mathrm{T}}$, where $(\cdot)^{\mathrm{T}}$ denotes transpose. A round bracket, as in $\boldsymbol{u}(t)$, denotes a sample of a continuous-time function, and a square bracket, as in $\boldsymbol{u}[h]$, denotes a sample of a discrete-time function. A subscript, as in $\boldsymbol{u}_k$, identifies the k^{th}-order perturbation elements. A superscript within round brackets, as in $\boldsymbol{u}^{(\nu)}$, identifies the ν^{th} DSCM sub-carrier elements with respect to the DSCM sub-carrier of interest. The 2×2 identity matrix is represented as $\boldsymbol{I}$ and the imaginary unit, $\sqrt{-1}$, is denoted as j. Furthermore, $(\cdot)^{\dagger}$ denotes Hermitian transpose, $|\cdot|^2$ denotes the Euclidean norm, and $\odot$ denotes the element-wise multiplication of vectors.

II. System Model

The PM-DSCM-WDM system model considered in this work is shown in Fig. 1. It provides a detailed illustration of the process involved in the x-polarization of a single WDM channel at the transmitter and a selected DSCM sub-carrier of interest (SCOI) at the receiver.

A. Transmitter

At the transmitter, the information bits of both polarizations of the WDM COI are independently modulated and split into parallel data streams, which correspond to the number of

DSCM sub-carriers. The pre-nonlinearity compensation is then applied to the data symbols for the schemes which consider a pre-nonlinearity compensation. Following that, the symbols pass through a pulse-shaping filter and are pre-compensated for 50% of the CD effects. Next, the signals are assigned to each DSCM sub-carrier and multiplexed to generate the DSCM signal. The DSCM signals are converted into the optical domain and multiplexed as the WDM signal. Finally, both polarizations of the WDM signal are combined to generate a PM signal, which is amplified to the transmission power and forwarded via the fiber.

B. Channel Propagation Model

The Manakov-PMD equation is a well-known nonlinear partial differential equation to model the PM signal propagation in the optical fiber channel [34]. The envelope of the PM signal at time t propagating at distance z, denoted as $\boldsymbol{u}(z,t) = [u(z,t) \text{ of } \mathrm{x}-\mathrm{pol}, u(z,t) \text{ of } \mathrm{y}-\mathrm{pol}]^{\mathrm{T}}$, is given by

$$\frac{\partial}{\partial z}\boldsymbol{u}(z,t) - \Delta\beta_1 \boldsymbol{\Sigma}(z)\frac{\partial}{\partial t}\boldsymbol{u}(z,t) + \mathrm{j}\frac{\beta_2}{2}\frac{\partial^2}{\partial t^2}\boldsymbol{u}(z,t) = \mathrm{j}\frac{8}{9}\gamma\left|\boldsymbol{u}(z,t)\right|^2\boldsymbol{u}(z,t)f(z) + \boldsymbol{n}(z,t), \tag{1}$$

where $\Delta\beta_1$ is the differential group delay between the two polarizations along the principal state of polarization, $\boldsymbol{\Sigma}(z)$ is the principal state of polarization rotation at distance z, β_2 is the chromatic dispersion coefficient, γ is the nonlinear coefficient, $f(z) = \exp(-\alpha \mod (z, L_{\mathrm{s}}))$ is the normalized attenuation profile of the fiber, where α is the attenuation coefficient, and L_{s} is the span length of the fiber, and $\boldsymbol{n}(z,t)$ is the amplified spontaneous emission (ASE) noise due to erbium-doped fiber amplifiers (EDFAs). In our simulation setup, the evolution of the PM signal envelope inside the optical fiber is obtained by numerically solving the Manakov-PMD equation using the split-step Fourier method (SSFM). At each step, following the SSFM algorithm, we apply the linear and nonlinear distortions independently and the fiber attenuation. The PMD effects are introduced according to the model in [35]. At the end of each span, the signal is amplified to compensate for the attenuation, and the ASE noise is added to the signal.

C. Receiver

At the receiver, both polarizations of the received signal are split and processed in parallel. Each polarization signal is first filtered for the WDM COI in the optical domain and then filtered for the DSCM SCOI in the digital domain. The resultant signal is then compensated for the remaining CD, and a matched filter to the transmitted pulse shape is applied. Then, the polarization mode dispersion effects are jointly compensated for both polarizations. Following that, the carrier phase mismatches are resolved and the nonlinearity compensation for SPM and iXPM effects are performed in two steps. The SPM compensation considers both polarizations of the DSCM SCOI, and the iXPM compensation assumes the knowledge of adjacent sub-carriers. Finally, the received symbols are demodulated, and the performance is evaluated using the Q^2-factor as the metric for comparison. The Q^2-factor in dB is calculated as $\mathrm{Q}^2 = 20\log_{10}(\sqrt{10}\,\mathrm{erfc}^{-1}(\frac{8\,\mathrm{BER}}{3}))$, where BER represents the bit error rate (BER) [30].

III. Joint SRO and Post-PB-NLC

In this section, we first derive the post-PB-NLC for the considered system and compute its computational complexity. Then, we describe the procedure of optimizing joint SRO and post-PB-NLC.

A. Post-PB-NLC for Pre-CDC Transmission

The proposed post-PB-NLC technique extends the compensation for SPM effects in conjunction with pre-CDC developed in [15] to SPM and iXPM compensation for the considered PM-DSCM-WDM system. For the iXPM compensation, we leverage the XPM compensation principles established in [21], [36]. We note that no prior research has investigated the influence of pre-CDC on the compensation of XPM or iXPM effects. We relegate the detailed derivations of the perturbation analysis to Appendix A.

For the SPM compensation, we approximate the received sample at the h^{th} time index in the SCOI (index zero) $\boldsymbol{b}^{(0)}[h]$ in (28) by ignoring the iXPM distortion terms as

$$\boldsymbol{b}^{(0)}[h] \approx \boldsymbol{a}^{(0)}[h] + \mathrm{j}\frac{8}{9}\gamma\sum_{m}\sum_{n}\boldsymbol{a}^{(0)\dagger}[h+m+n] \times \boldsymbol{a}^{(0)}[h+m]\boldsymbol{a}^{(0)}[h+n]C^{(0)}_{m,n}, \tag{2}$$

where $\boldsymbol{a}^{(\nu)}[h]$ is the transmitted symbol at the h^{th} time index in the ν^{th} sub-carrier, and $C^{(\nu)}_{m,n}$ is the perturbation coefficient for the ν^{th} sub-carrier provided in (29) with $L_{\mathrm{c}} = L/2$ for the considered 50% pre-CDC transmission, and L is the transmission length. Then, we adopt the additive-multiplicative model from [37] to obtain the SPM compensated sample at the SCOI as

$$\boldsymbol{b}'^{(0)}[h] = \left(\boldsymbol{b}^{(0)}[h] - \boldsymbol{\Delta}^{(0)}[h]\right) \odot \exp\left(-\mathrm{j}\boldsymbol{\Phi}^{(0)}[h]\right), \tag{3}$$

where the additive and multiplicative correction terms are given by

$$\boldsymbol{\Delta}^{(0)}[h] = \mathrm{j}\frac{8}{9}\gamma\sum_{m\neq 0}\sum_{n\neq 0}\boldsymbol{a}'^{(0)\dagger}[h+m+n] \times \boldsymbol{a}'^{(0)}[h+m]\boldsymbol{a}'^{(0)}[h+n]C^{(0)}_{m,n}, \tag{4}$$

and

$$\boldsymbol{\Phi}^{(0)}[h] = \frac{8}{9}\gamma\sum_{m=0}\sum_{n}\left|\boldsymbol{a}'^{(0)}[h+m+n]\right|^2 C^{(0)}_{m,n} + \frac{8}{9}\gamma\sum_{m\neq 0}\sum_{n=0}\left|\boldsymbol{a}'^{(0)}[h+m+n]\right|^2 C^{(0)}_{m,n}. \tag{5}$$

During the compensation at the receiver, we approximate the transmit symbols $\boldsymbol{a}^{(\nu)}[h]$ with the hard-decision decoded received symbols $\boldsymbol{a}'^{(\nu)}[h]$ in (4) and (5).

For the iXPM compensation, we assume that SPM is fully compensated. Therefore, using (28), we approximate the SPM

compensated sample as

$$\boldsymbol{b'}^{(0)}[h] \approx \boldsymbol{a}^{(0)}[h] + \mathrm{j}\frac{8}{9}\gamma \sum_{\nu\neq 0}\sum_{m}\sum_{n}\Big(\boldsymbol{a}^{(\nu)\dagger}[h+m+n] \times \boldsymbol{a}^{(\nu)}[h+m]\boldsymbol{I} + \boldsymbol{a}^{(\nu)}[h+m]\boldsymbol{a}^{(\nu)\dagger}[h+m+n]\Big) \times \boldsymbol{a}^{(0)}[h+n]C^{(\nu)}_{m,n}. \quad (6)$$

Then, by again utilizing the additive-multiplicative model, we obtain the iXPM compensated sample at the SCOI as

$$\boldsymbol{b''}^{(0)}[h] \approx \Big(\boldsymbol{b'}^{(0)}[h] - \boldsymbol{\Delta'}^{(0)}[h]\Big) \odot \exp\Big(-\mathrm{j}\boldsymbol{\Phi'}^{(0)}[h]\Big), \quad (7)$$

where

$$\boldsymbol{\Delta'}^{(0)} = \mathrm{j}\frac{8}{9}\gamma \sum_{\nu\neq 0}\sum_{m}\sum_{n\neq 0}\Big(\boldsymbol{a'}^{(\nu)\dagger}[h+m+n] \times \boldsymbol{a'}^{(\nu)}[h+m]\boldsymbol{I} + \boldsymbol{a'}^{(\nu)}[h+m] \times \boldsymbol{a'}^{(\nu)\dagger}[h+m+n]\Big)\boldsymbol{a'}^{(0)}[h+n]C^{(\nu)}_{m,n}, \quad (8)$$

and

$$\boldsymbol{\Phi'}^{(0)}[h] = \frac{8}{9}\gamma \sum_{\nu\neq 0}\sum_{m}\sum_{n=0}\Big(\boldsymbol{a'}^{(\nu)\dagger}[h+m+n] \times \boldsymbol{a'}^{(\nu)}[h+m]\boldsymbol{I} + \boldsymbol{a'}^{(\nu)}[h+m] \times \boldsymbol{a'}^{(\nu)\dagger}[h+m+n]\Big) C^{(\nu)}_{m,n}. \quad (9)$$

B. Complexity of Post-PB-NLC

One of the advantages of PB-NLC is the ability to compute the perturbation coefficient $C^{(\nu)}_{m,n}$ offline [21]. Furthermore, the hard-decision symbol multiplications can be stored in a lookup table and reused for the computation [20]. Hence, the computational complexity of the proposed PB-NLC technique is approximately equal to the multiplications required to compute the additive and multiplicative terms $\boldsymbol{\Delta}^{(0)}[h]$, $\boldsymbol{\Phi}^{(0)}[h]$, $\boldsymbol{\Delta'}^{(0)}[h]$, and $\boldsymbol{\Phi'}^{(0)}[h]$ in (4), (5), (8), and (9), respectively. This in turn means that the number of perturbation coefficients is a meaningful proxy for computational complexity. We limit the number of coefficients by selecting a subset of significant coefficients with the largest absolute values and by selecting a limited number of adjacent sub-carriers for iXPM compensation.

Fig. 2 compares the absolute values of the perturbation coefficients for transmission with and without pre-CDC. The coefficients are normalized with respect to the peak value of the SPM coefficients with pre-CDC, and a truncation threshold of -45 dB is applied to select the significant coefficients. The results are presented for a 20×80 km link, 12 GBd sub-carrier symbol rate with RRC pulses using roll-off factor 0.1, and 13.8 GHz sub-carrier spacing. Fig. 2(a) and (b) compare the perturbation coefficients for SPM compensation without and with half-length pre-CDC, respectively. Pre-CDC results in an approximately three-fold reduction in the number of coefficients that meet the given threshold and thus reduces the complexity of SPM compensation significantly. This finding is similar to [15]. Fig. 2(c) and (d) show the magnitude perturbation coefficients for iXPM (originating from one adjacent sub-carrier) without and with pre-CDC, respectively. We observe a small reduction in the number of perturbation coefficients by applying the pre-CDC. Thus, the observations from Fig. 2 indicate that PB-NLC with joint SPM and iXPM compensation enjoys a computational complexity reduction when applied in conjunction with pre-CDC. While the additional reduction in complexity for iXPM is less substantial than that for SPM, it is important to establish that the computational burden is further reduced rather than increased.

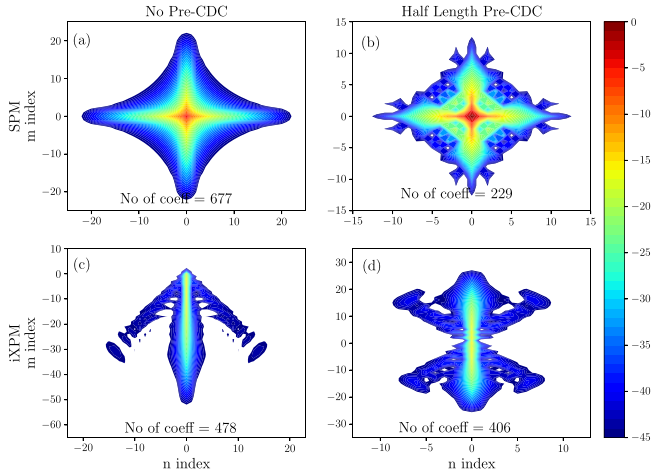

Fig. 2. Comparison of SPM and iXPM perturbation coefficients for the transmission without pre-CDC on the left and with half-length ($L_c = L/2$) pre-CDC from (29) on the right. Absolute values in dB relative to the strongest coefficient value for SPM with pre-CDC.

The SPM and iXPM perturbation coefficients, with half-length pre-CDC and RRC pulse shaping, exhibit a relationship $C^{(0)}_{m,n} = C^{(0)}_{-m,-n} = -C^{(0)^*}_{m,-n} = -C^{(0)^*}_{-m,n}$ and $C^{(\nu)}_{m,n} = -C^{(\nu)^*}_{m,-n}$, respectively [15]. This relationship allows us to group (add) real and imaginary parts of the symbol triplet corresponding to the same real and imaginary parts of perturbation coefficients, and then multiply them. Such a grouping technique provides a reduction in computational complexity without any performance degradation [15]. Additional complexity reduction with minimal performance degradation can be attained through quantization of perturbation coefficients [30]. We collect all the perturbation coefficients (SPM and iXPM) for the system configuration. Then, we apply the k-means clustering algorithm to approximate similar perturbation coefficients using specific complex numbers known as centroids. The centroids act as a proxy for perturbation coefficients, enabling us to group real and imaginary parts of the symbol triplet corresponding to the real and imaginary parts of centroids obtained with quantization. This process effectively decreases the number of required multiplications and lowers the computational complexity. In this paper, we measure the complexity in terms of the number of real multiplications considering the grouping technique. Additionally, we provide complexity with quantization where explicitly stated.

C. Joint SRO and PB-NLC Optimization

As discussed in Section I, the various nonlinear impairments exhibit distinct behaviors in relation to the sub-carrier symbol rate [12]. Consequently, a symbol rate exists that minimizes the overall impact of nonlinear distortions. At the same time, the effectiveness and computational complexity of post-PB-NLC hinge on the number of significant perturbation coefficients, which is inherently linked to the symbol rate of the DSCM sub-carriers. Hence, we observe an interplay between symbol rate and nonlinear effects as well as between symbol rate and nonlinearity compensation. The existing literature, as outlined in [27], overlooks the aforementioned interplay due to its utilization of DBP, which uniformly addresses all nonlinear effects and remains independent of symbol rate. Additionally, it is noteworthy that there has been no prior investigation into the interaction between symbol rate and symbol rate-dependent nonlinearity compensation within DSCM systems. This motivates the optimization of joint SRO and PB-NLC in the context of PM-DSCM-WDM transmission.

Our approach to map out the performance and complexity trade-off for joint SRO and post-PB-NLC in conjunction with pre-CDC is as follows. We define a meaningful range of symbol rates for the DSCM sub-carriers that will be considered for SRO, e.g., in Section V. We then calculate the perturbation coefficients associated with each symbol rate using (29). We conduct numerical simulations for the PM-DSCM-WDM system with different DSCM sub-carrier symbol rates and apply post-PB-NLC for the pre-CDC transmission. We leverage the adaptability of PB-NLC to address nonlinear effects, ranging from solely SPM effect, SPM and a limited amount of iXPM effects, and extending to encompass SPM alongside all iXPM effects. This strategy paves the way to explore the relationship between the compensated nonlinear effects and symbol rates, a gap evident in the existing literature. The resulting Q^2-factor is the measure of performance. Finally, we compute the computational complexity as described in Section III-B.

IV. Split PB-NLC

In this section, we discuss our proposed split PB-NLC technique for pre-CDC transmission in PM-DSCM-WDM systems. This technique pre-compensates the iXPM effects associated with the signal propagation along the first half of the fiber link in the pre-NLC block of the transmitter shown in Fig. 1. The whole SPM effect and the iXPM effects associated with the signal propagation along the second half of the fiber link are compensated at the receiver. In the following, we discuss the details of deriving the iXPM pre- and post-compensation, the complexity of split PB-NLC, and the advantages of split PB-NLC. The SPM compensation remains the same as in Section III.

A. The iXPM Pre-Compensation

To obtain the pre-compensation at the transmitter, we follow the steps in Appendix A assuming the signal propagates a distance of $L/2$. This results in similar solution in (28), where we have different perturbation coefficients, denoted by $\bar{C}^{(\nu)}_{m,n}$, that are obtained by replacing the upper integral limit of (30) by $z = L/2$. Then, for the iXPM pre-compensation, we can represent the equivalent received sample at the end of the first half-length propagation by neglecting the SPM distortion terms as

$$\tilde{\boldsymbol{b}}'^{(0)}[h] \approx \boldsymbol{a}^{(0)}[h] + \mathrm{j}\frac{8}{9}\gamma \sum_{\nu\neq 0}\sum_{m}\sum_{n}\Big(\boldsymbol{a}^{(\nu)^\dagger}[h+m+n] \times \boldsymbol{a}^{(\nu)}[h+m]\boldsymbol{I} + \boldsymbol{a}^{(\nu)}[h+m]\boldsymbol{a}^{(\nu)^\dagger}[h+m+n]\Big) \times \boldsymbol{a}^{(0)}[h+n]\bar{C}^{(\nu)}_{m,n}. \tag{10}$$

The pre-compensation is performed at the transmitter by replacing the original data symbol $\boldsymbol{a}^{(0)}[h]$ for the SCOI with

$$\bar{\boldsymbol{a}}^{(0)}[h] = \boldsymbol{a}^{(0)}[h] - \boldsymbol{\Delta}^{\prime\prime(0)}[h], \tag{11}$$

where $\boldsymbol{\Delta}^{\prime\prime(0)}[h]$ is the second additive term in (10).

B. The iXPM Post-Compensation

The iXPM pre-compensated symbols are passed through the transmitter block, which also performs 50% pre-CDC, and then transmitted through the fiber. When the symbols propagate to the midpoint at $z = L/2$, the effects of the CD and iXPM pre-compensation will have been reversed by the dispersion and iXPM effects during the propagation. At this point, we still experience SPM effects, which become less significant though for DSCM systems with a small sub-carrier symbol rate. Further, the SPM effect accumulated during the first half of fiber does not impact the first-order approximation for the second-half propagation [38]. It contributes only to the higher-order nonlinearity during the propagation of the second half of fiber. Thus, we compute the iXPM compensation at the receiver by assuming that the original transmit symbols propagate from the midpoint ($z = L/2$) to the receiver ($z = L$). Therefore, at the receiver, we approximate the signal after SPM compensation as

$$\boldsymbol{b}'^{(0)}[h] = \boldsymbol{a}^{(0)}[h] + \mathrm{j}\frac{8}{9}\gamma \sum_{f\neq 0}\sum_{m}\sum_{n}\Big(\boldsymbol{a}^{(\nu)^\dagger}[h+m+n] \times \boldsymbol{a}^{(\nu)}[h+m]\boldsymbol{I} + \boldsymbol{a}^{(\nu)}[h+m]\boldsymbol{a}^{(\nu)^\dagger}[h+m+n]\Big) \times \boldsymbol{a}^{(0)}[h+n]\bar{\bar{C}}^{(\nu)}_{m,n}, \tag{12}$$

where $\bar{\bar{C}}^{(\nu)}_{m,n}$ are the perturbation coefficients corresponding to the second half of the propagation. These are obtained by setting the integration limits of the nonlinear kernel in (30) from $z = L/2$ to $z = L$.

From (12) and additive-multiplicative model in [37], the iXPM post-compensated received symbol is obtained as

$$\boldsymbol{b}''^{(0)}[h] = \Big(\boldsymbol{b}'^{(0)}[h] - \boldsymbol{\Delta}'''^{(0)}[h]\Big) \odot \exp\Big(-\mathrm{j}\boldsymbol{\Phi}'''^{(0)}[h]\Big), \tag{13}$$

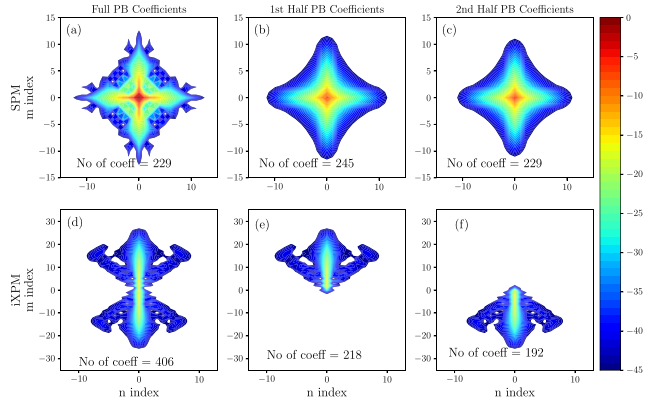

Fig. 3. A comparison of SPM and iXPM perturbation coefficients for a 50% pre-CDC transmission corresponding to full-length ($C^{(\nu)}_{m,n}$), first half-length ($\bar{C}^{(\nu)}_{m,n}$) and second half-length ($\bar{\bar{C}}^{(\nu)}_{m,n}$) of the fiber link.

where

$$\boldsymbol{\Delta}^{\prime\prime\prime(0)}[h] = \mathrm{j}\frac{8}{9}\gamma \sum_{\nu\neq 0}\sum_{m}\sum_{n\neq 0}\Big(\boldsymbol{a}'^{(\nu)\dagger}[h+m+n] \times \boldsymbol{a}'^{(\nu)}[h+m]\boldsymbol{I} + \boldsymbol{a}'^{(\nu)}[h+m] \times \boldsymbol{a}'^{(\nu)\dagger}[h+m+n]\Big)\boldsymbol{a}'^{(0)}[h+n]\bar{\bar{C}}^{(\nu)}_{m,n} \quad (14)$$

and

$$\boldsymbol{\Phi}^{\prime\prime\prime(0)}[h] = \frac{8}{9}\gamma \sum_{\nu\neq 0}\sum_{m}\sum_{n=0}\Big(\boldsymbol{a}'^{(\nu)\dagger}[h+m+n] \times \boldsymbol{a}'^{(\nu)}[h+m]\boldsymbol{I} + \boldsymbol{a}'^{(\nu)}[h+m] \times \boldsymbol{a}'^{(\nu)\dagger}[h+m+n]\Big)\bar{\bar{C}}^{(\nu)}_{m,n}. \quad (15)$$

C. Complexity of Split PB-NLC

The SPM and first adjacent sub-carrier iXPM perturbation coefficients for full-length, first half-length, and second half-length of the fiber link are shown in Fig. 3. The perturbation coefficients are normalized by the peak value of full-length SPM coefficients and a truncation threshold of -45 dB is applied to the normalized coefficients. Again, the results are presented for a 20×80 km link with lumped amplified, 12 GBd sub-carrier symbol rate with RRC pulses using roll-off factor 0.1, and 13.8 GHz sub-carrier spacing transmission. We observe similar numbers of the full-length, first-half-length, and second-half-length SPM coefficients. However, the numbers of full-length iXPM coefficients are approximately divided into first-half and second-half iXPM coefficients. This is not a coincidence but a fundamental property of iXPM that is exploited in split PB-NLC as explained in Appendix B. Therefore, the selection of first half-length pre-iXPM compensation at the transmitter and second half-length post-iXPM compensation at the receiver, together with full-length SPM compensation at the receiver enables us to use the minimum number of perturbation coefficients as given in Fig. 3(a), (e), and (f). Thus, the receiver side post-iXPM compensation complexity is reduced by a factor of two while the overall complexity of nonlinearity compensation remains the same as in Section III.

The split PB-NLC perturbation coefficients for iXPM pre-compensation and iXPM post-compensation exhibit the relationships $C^{(\nu)}_{m,n} = -C^{(\nu)^*}_{m,-n}$, as seen in the post-PB-NLC. The groupings, initially identified in post-PB-NLC, persist in split PB-NLC despite splitting the perturbation compensation process into two parts. Therefore, the grouping technique proportionally reduces the computational complexity of both post-PB-NLC and split PB-NLC.

On the other hand, quantization affects the computational complexity of post-PB-NLC and split PB-NLC differently. The reduction in computational complexity achieved through quantization depends on the number of centroids used in the quantization process. Before quantization, the perturbation coefficients of post-PB-NLC have distinct complex values for the first and second halves of propagation. During quantization, similar perturbation coefficients are approximated with centroids. If a large number of centroids are employed, those centroids remain close to the original perturbation coefficients and distinct for both halves of propagation. However, when the number of centroids is reduced, the same centroid is required to represent the perturbation coefficients from both halves. Consequently, when the perturbation compensation is divided between transmitter and receiver in split PB-NLC, this common centroid necessitates two computations, one at the transmitter and one at the receiver. Thus, when the number of centroids decreases, the effectiveness of split PB-NLC in reducing the computational complexity at the receiver decreases, as demonstrated in Section V-E.

D. Advantages of Split PB-NLC

We identify three advantages of split PB-NLC for a 50% pre-CDC transmission. Firstly, as illustrated in Fig. 2(c) and (d), the introduction of pre-CDC does not provide a significant reduction in the number of iXPM perturbation coefficients, unlike its effect on SPM. However, as it is shown in Appendix B, the 50% pre-CDC together with dispersion effects and the walk-off between SCOI and adjacent sub-carriers create distinct sets of triplets that contribute to the iXPM distortions of the first and the second half of the link. This phenomenon creates the possibility of performing the first half of the iXPM compensation at the transmitter and the second half of the iXPM compensation at the receiver without repeating the same triplet multiplications with perturbation coefficients. Thus, overall iXPM computational complexity can evenly be distributed between the transmitter and receiver. It is worth noting that conventional iXPM compensation without pre-CDC does not possess the aforementioned property. In such a case, implementing split PB-NLC adds complexity due to pre-compensation at the transmitter, without a corresponding reduction in receiver complexity. The same observation applies to SPM compensation for pre-CDC transmission due to the absence of walk-off.

Secondly, the perturbation solution of the Manakov (19) provides the field at a distance L as $\boldsymbol{u}(z=L,t) =$

TABLE I
SIMULATION PARAMETERS FOR THE PM-DSCM-WDM SYSTEM

No of WDM channels	5
WDM channel symbol rate	48 GBd
WDM channel spacing	60 GHz
No of DSCM sub-carriers	24, 16, 12, 8, 6, 4, 2, 1
DSCM sub-carrier symbol rates	48 GBd/ No of DSCM sub-carriers
DSCM sub-carrier spacing	1.15 × DSCM sub-carrier symbol rates

TABLE II
SIMULATION PARAMETERS FOR THE OPTICAL FIBER

Parameter	Value and unit
Number of spans	20
Span length	80 km
CD	16 ps/nm/km
Gamma	1.4 $W^{-1}km^{-1}$
PMD	0.1 $ps/\sqrt{km}$
Fiber loss	0.2 dB/km
Center wavelength	1550 nm

$\sum_{k=0}^{\infty} \gamma^k \boldsymbol{u}_k(z=L,t)$, which is approximated by its zeroth-order and first-order terms for the derivation of PB-NLC (see Appendix A). Since higher-order nonlinear effects are not taken into account, this approximation is accurate when higher-order nonlinear effects are minimal. In a long-haul optical fiber, all the nonlinear effects accumulate over the length of the fiber. Thus, considering the half-length of the fiber reduces the unaccounted higher-order nonlinear effects to the half-length of the fiber and improves the accuracy of the first-order approximation.

Finally, split PB-NLC exploits the benefits of both full pre-PB-NLC and full post-PB-NLC techniques. The pre-PB-NLC approach leverages the knowledge of transmit symbols to calculate the PB-NLC with increased accuracy. However, it requires feedback to adapt to dynamic changes in the link. On the other hand, the post-PB-NLC method excels in adapting to dynamic link conditions by fine-tuning and optimizing compensation to address changes in the channel link [30]. Nevertheless, it relies on hard-decision decoded symbols for PB-NLC calculations, making it susceptible to errors introduced during the hard-decision decoding process, negatively impacting post-PB-NLC performance. The proposed split PB-NLC approach offers a balanced solution. It capitalizes on the precise pre-compensation of the first half of the link's iXPM effects using the known transmit symbols, also resulting in fewer errors in hard-decision decoded symbols used for the post-compensation. Furthermore, it can fine-tune and optimize post-compensation to handle dynamic link changes at the receiver.

V. RESULTS AND DISCUSSIONS

In this section, we present numerical results from simulations to highlight the optimization of joint SRO and PB-NLC for pre-CDC transmission and its benefits in a PM-DSCM-WDM system. We also showcase the advantages of split PB-NLC.

A. Simulation Parameters

We simulate the PM-DSCM-WDM system shown in Fig. 1 with different DSCM sub-carrier configurations as listed in Table I. We consider 64-ary quadrature amplitude modulation (64-QAM) and an RRC pulse shaping filter with a roll-off factor of 0.1. The pre-CDC block applies a 50% of CDC to the pulses. An EDFA at the transmitter sets the transmit signal power and in-line EDFAs with a 4.5 dB noise figure compensate for fiber attenuation losses. The optical fiber parameters are listed in Table II. The propagation via optical fiber is simulated with split-step Fourier method using 400 steps per span. At the receiver, the center channel of the five-channel WDM transmission is considered as the WDM COI. Firstly, the polarizations of the received field are separated and the WDM COI is filtered. Then, the DSCM SCOI is filtered, a 50% post-CDC is applied, a least mean square (LMS) adaptive 2×2 equalizer is used to compensate for PMD, and a pilot-based mean constant phase rotation is applied for carrier phase recovery (CPR). This is followed by the considered techniques for nonlinearity compensation. Finally, the signal is demodulated and Q^2-factor is computed to evaluate the performance. The DSCM sub-carriers exhibit different performances based on their positions within the WDM COI spectrum. Hence, the WDM COI performance is determined by averaging the BER of all the DSCM sub-carriers within the WDM COI.

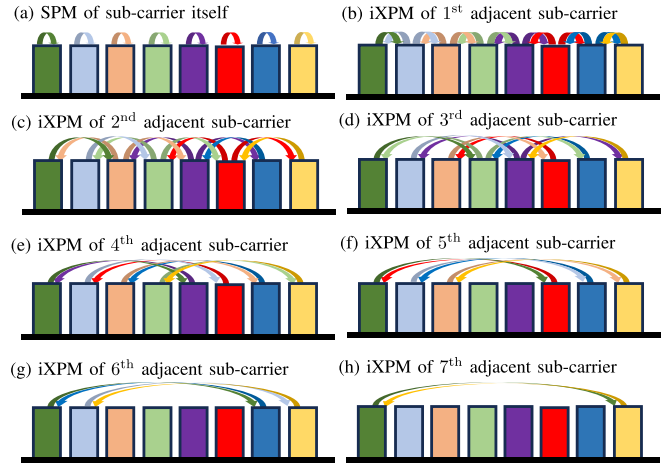

Fig. 4. Illustration of the SPM and iXPM effects present within WDM COI of (6 GBd×8) × 5 configuration of the PM-DSCM-WDM system.

B. Label Definitions

The (6 GBd×8) × 5 configuration of the PM-DSCM-WDM system consists of five WDM channels, each featuring eight DSCM sub-carriers with a sub-carrier symbol rate of 6 GBd. Fig. 4 illustrates the sub-carrier interactions in terms of SPM and iXPM due to ν^{th} adjacent DSCM sub-carrier present within a WDM COI for the (6 GBd×8) × 5 PM-DSCM-WDM system. Since PB-NLC can consider different numbers of adjacent DSCM sub-carriers for iXPM compensation, we introduce the following labels for clarity:

- CDC: This denotes no nonlinearity compensation, i.e., CDC only.
- DBP: This denotes DBP for the entire WDM COI.

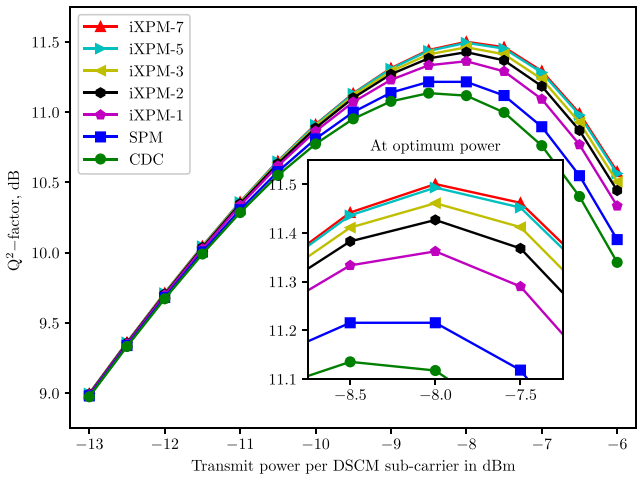

Fig. 5. Performance of post-PB-NLC in the (6 GBd×8) × 5 configuration of the PM-DSCM-WDM system.

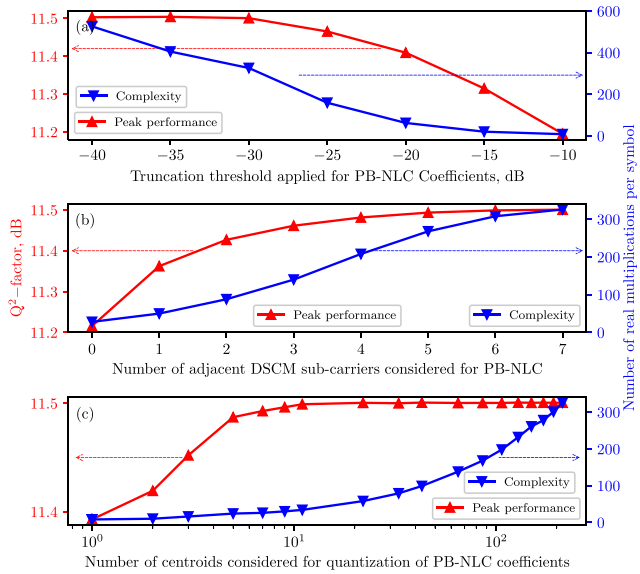

Fig. 6. Performance and computational complexity of post-PB-NLC in the (6 GBd×8) × 5 configuration of the PM-DSCM-WDM system.

- SPM: This technique compensates for the linear effects and the SPM effects highlighted in Fig. 4(a).
- iXPM-ν: This PB-NLC technique compensates for linear effects, SPM effects, and iXPM effects from up to ν^{th} adjacent sub-carriers. For example, iXPM-2 compensates for the linear effects, SPM effects shown in Fig. 4(a), and the iXPM effects shown in Fig. 4(b) and (c).
- iXPM-Full: This PB-NLC technique compensates for linear effects, SPM effects, and iXPM effects caused by all adjacent sub-carriers within the WDM COI, i.e., all the interactions identified in Fig. 4 for the 6 GBd×8 DSCM configuration.

C. Characteristics of Post-PB-NLC in PM-DSCM-WDM Systems

In this section, we illustrate the characteristics of post-PB-NLC for SPM and iXPM compensation in PM-DSCM-WDM transmission. We do so by evaluating its performance in relation to key factors such as transmit power, the number of adjacent DSCM sub-carriers considered for the PB-NLC, and the truncation threshold employed for the PB-NLC. This analysis is insightful in its own right, and it sets the stage for the optimization of joint nonlinearity mitigation and compensation addressed in the next section.

Fig. 5 shows the average Q^2-factor performance for the WDM COI in the (6 GBd×8) × 5 configuration of the PM-DSCM-WDM system. The performance is examined with respect to the transmit power per DSCM sub-carrier. The inset figure shows a closer look at the performance around the optimum transmit power. The different curves listed in the legends correspond to the number of adjacent DSCM sub-carriers considered in PB-NLC, i.e., the extent to which nonlinearity within the WDM COI is compensated. PB-NLC uses the significant perturbation coefficients that meet the truncation threshold of −30 dB compared to the maximum SPM perturbation coefficient. Later, we show that a truncation threshold below −30 dB does not provide significant performance gains. We observe from Fig. 5 that the performance of CDC exhibits a linear increase with transmit power at low transmit power regions. However, as the transmit power increases, the performance gradually decreases due to the prevailing nonlinear effects. PB-NLC does not impart any distinguishable impact within the linear regime. Its benefits manifest in the performance gains within the nonlinear regime. Notably, the iXPM-Full technique, which compensates for linear, SPM, and all iXPM effects within the WDM COI, achieves a PB-NLC gain of 0.36 dB compared to linear compensation in the considered (6 GBd×8) × 5 PM-DSCM-WDM system. Moreover, the performance of PB-NLC improves as the number of adjacent DSCM sub-carriers considered for iXPM compensation increases. However, it is noteworthy to emphasize that the magnitude of these performance improvements progressively diminishes as the considered adjacent DSCM sub-carriers are positioned further away from the DSCM SCOI.

The performance and complexity of PB-NLC in conventional WDM systems can be controlled by using a truncation threshold and selecting the most significant perturbation coefficients that meet the truncation threshold. The PB-NLC in the DSCM-WDM system has an additional degree of freedom to control the performance and complexity by selecting the number of adjacent channels to compensate for their iXPM effects. On top of that, the quantization technique can be applied to further reduce the complexity. The integration of DSCM and PB-NLC provides a comprehensive approach to regulate the performance and complexity of the PM-DSCM-WDM system, as depicted in Fig. 6.

Fig. 6(a) illustrates the average performance of the WDM COI at the optimum transmit power and the corresponding computational complexity to perform post-PB-NLC as a function of the truncation threshold for the (6 GBd×8) × 5 PM-DSCM-WDM system. For these results, post-PB-NLC (iXPM-7) is performed using only the perturbation coefficients that exceed

the truncation threshold values on the horizontal axis. Clearly, as the truncation threshold increases, the number of perturbation coefficients meeting the selection criterion decreases and consequently, post-PB-NLC is performed with a reduced number of perturbation coefficients. Fig. 6(a) highlights the resulting trade-off between the decline in performance and the reduction in computational complexity of the nonlinearity compensation technique. Moreover, we observe that including perturbation coefficients that are below the -30 dB truncation threshold does not result in significant performance improvements.

Fig. 6(b) shows the average performance of the WDM COI at optimum transmit power and the corresponding computational complexity to perform post-PB-NLC as a function of the considered number of adjacent sub-carriers. For these results, the perturbation coefficients above the -30 dB threshold are used for PB-NLC. As expected, we observe that performance improves as the number of adjacent sub-carriers considered for PB-NLC increases. However, the rate of performance improvement diminishes with the inclusion of additional adjacent sub-carriers. This suggests that the nearest sub-carriers have a more substantial impact on iXPM effects, while the influence of the farthest sub-carriers is negligible. The complexity displays a sigmoid-like pattern. This pattern arises majorly due to the variation of interfering terms added by the adjacent sub-carriers. For instance, in a 6 GBd$\times$8 DSCM configuration, SPM to iXPM-1 adds 14 interference terms, as shown in Fig. 4(b), while the iXPM-6 to iXPM-7 adds only two additional interference terms, as shown in Fig. 4(h).

Fig. 6(c) demonstrates the average performance of the WDM COI at optimum transmit power and the corresponding computational complexity to perform post-PB-NLC as a function of the considered number of centroids used in quantization technique. First, we select the perturbation coefficients above the -30 dB threshold. Then, we combine SPM and iXPM coefficients and quantize them to the given number of centroids in the x-axis. Then, we compute the additive and multiplicative terms for the post-PB-NLC using the quantized coefficients. We enforce the constraint that quantized multiplicative perturbation coefficients are strictly imaginary, while quantized additive perturbation coefficients are complex. The results suggest that the performance of PB-NLC remains stable when a large number of centroids are employed during quantization. Conversely, performance degradation is observed as the number of centroids considered for quantization decreases, particularly evident with fewer centroids. Additionally, the computational complexity of post-PB-NLC displays exponential growth relative to the number of centroids utilized. Taken together, the analysis of both curves demonstrates that quantization can significantly reduce the computational complexity of post-PB-NLC without inducing significant performance degradation.

Our investigation into PB-NLC within PM-DSCM-WDM systems provides comprehensive insights into performance and complexity, guiding informed decision-making for the practical implementation of PB-NLC in various aspects such as perturbation coefficient selection, adjacent sub-carriers selection, and quantization. Furthermore, it facilitates useful decisions during the design process of joint SRO and PB-NLC within PM-DSCM-WDM systems.

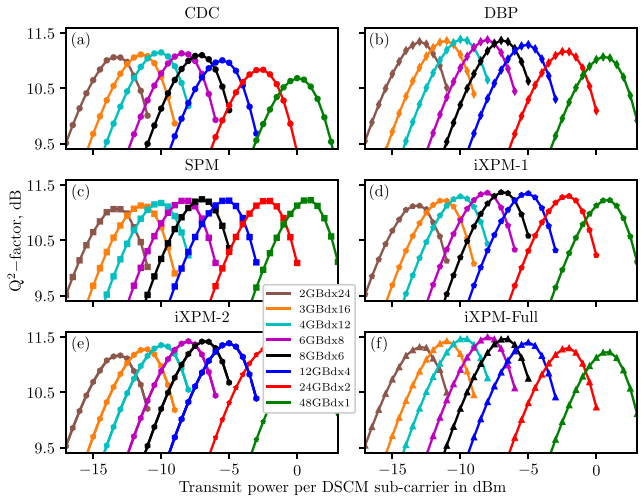

Fig. 7. Symbol rate optimization for CDC, DBP, and post-PB-NLC in the 48 GBd$\times$5 PM-DSCM-WDM system with different numbers of DSCM sub-carriers and different nonlinearity compensation schemes.

D. Joint SRO and Post-PB-NLC for PM-DSCM-WDM Systems

We now turn to the joint operation of SRO for nonlinearity mitigation and post-PB-NLC for nonlinearity compensation. SRO with CDC and SRO with DBP from [27] are considered as benchmark schemes.

To investigate the joint SRO and post-PB-NLC technique for the PM-DSCM-WDM system, we examine the performance for various numbers of DSCM sub-carriers and their corresponding symbol rates as listed in Table I, following the procedure described in Section III-C. Fig. 7(a)–(f) show the corresponding average performances for the WDM COI using CDC, DBP, SPM, iXPM-1, iXPM-2, and iXPM-Full compensation, respectively, as functions of the transmit power per DSCM sub-carrier. The considered PB-NLC techniques have been shown to provide distinguishable performance gains in Fig. 5, and they are implemented with coefficients exceeding the -30 dB threshold based on the results in Fig. 6. DBP performs backpropagation of the whole WDM COI with two samples per symbol and one step per span. We observe that joint SRO and nonlinearity compensation is effective in that additional gains are realized for all compensation techniques considered in Fig. 7(a)–(f). Upon closer examination, we make a noteworthy observation: the peak performance with different PB-NLC techniques is achieved at different DSCM sub-carrier symbol rates, unlike what is reported in the existing literature with CDC and DBP.

To highlight the performance differences associated with DSCM sub-carrier symbol rates, we separate the peak performances of each curve in Fig. 7 and plot them along with their corresponding computational complexities in Fig. 8. The performances of all the considered techniques initially increase with the DSCM sub-carrier symbol rate and then diminish for a higher

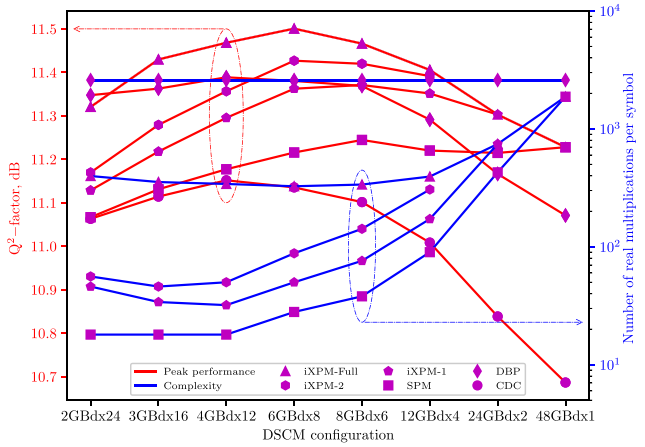

Fig. 8. Performance and computational complexity of PB-NLC with different DSCM sub-carrier symbol rates in the PM-DSCM-WDM system compared to CDC and DBP.

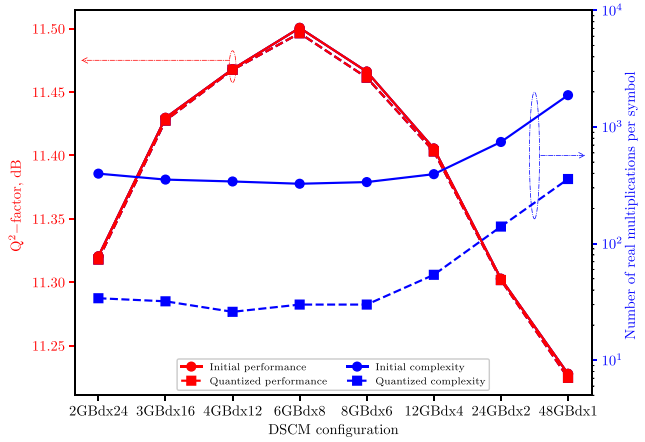

Fig. 9. Peak performance and computational complexity of iXPM-Full before and after quantization for different DSCM sub-carrier symbol rates in the PM-DSCM-WDM system.

sub-carrier symbol rate. That is, there is an optimal sub-carrier symbol rate, as it is known from the case with nonlinearity compensation [13]. The complexity of single step per span DBP is calculated as $N_{\mathrm{s}}(4N_{\mathrm{F}}\log_2(N_{\mathrm{F}})+10.5N_{\mathrm{F}})/N$, where N_{s} is the number of spans, N_{F} is the FFT size and N is the effective number of symbols neglecting overlaps between FFT frames [39]. The DBP complexity remains the same regardless of the DSCM configuration since it performs DBP on the WDM COI in all cases. The PB-NLC complexities slightly decrease with the DSCM sub-carrier symbol rates and then sharply increase for the higher DSCM sub-carrier symbol rates. This trend shows the remaining nonlinear effects after the nonlinear mitigation by using SRO. Interestingly, the complexity of iXPM-Full is at its minimum when it attains peak performance. This observation is novel in comparison to existing literature and underscores that the joint SRO and post-PB-NLC for DSCM-WDM systems simultaneously *mitigate* the nonlinear effects and then efficiently *compensate* for the residual nonlinear effects. Notably, the joint SRO and post-PB-NLC iXPM-Full achieves a 0.25 dB Q^2-factor gain and a six times reduction in complexity for the $(6\mathrm{GBd}\times 8)\times 5$ PM-DSCM-WDM system, in comparison to the simplistic $(48\mathrm{GBd}\times 1)\times 5$ WDM system.

CDC and DBP attain their peak performances at the same DSCM sub-carrier symbol rate (4 GBd), which is consistent with the results in [27]. However, the peaks shift to higher DSCM sub-carrier symbol rates of 6 GBd for iXPM-Full and iXPM-2 and 8 GBd for iXPM-1 and SPM. This trend can be explained by considering the compensation of nonlinear effects. CDC does not address nonlinear interference. DBP attempts to compensate SPM, iXPM, and iFWM effects evenly, to the extent possible with a one-step-per-span backpropagation. This leads to the same optimal DSCM sub-carrier symbol rate as for CDC. On the other hand, iXPM-Full tackles SPM and iXPM but does not consider iFWM effects. Therefore, the optimum symbol rate shifts to a higher DSCM sub-carrier symbol rate, with fewer sub-carriers that have a lesser impact due to iFWM. Furthermore, with iXPM-2 and iXPM-1, we compensate for SPM and iXPM effects within a limited sub-band of the WDM COI. As a result, these techniques achieve peak performance by balancing the presence of iXPM effects and the amount of iXPM compensated. When it comes to SPM compensation, it is expected to yield a peak for the largest sub-carrier symbol rate. However, the limitation imposed by a truncation threshold on SPM compensation leaves residual SPM effects after the compensation. Thus, the resulting peak sub-carrier symbol rate is lower than the largest DSCM sub-carrier symbol rate. In summary, the optimum DSCM sub-carrier symbol rate depends on which nonlinear effects are compensated and the extent to which they are compensated. Therefore, our results provide important information for selecting symbol rates based on nonlinearity compensation, enabling effective implementation of joint nonlinearity mitigation and compensation. Thus, practical implementations involving SRO and PB-NLC within PM-DSCM-WDM systems can exploit performance gains at no additional cost by selecting the appropriate DSCM symbol rate according to the limitations of PB-NLC to access adjacent sub-carriers.

Fig. 9 illustrates the complexity reduction achieved with quantization for different DSCM sub-carrier symbol rates in the PM-DSCM-WDM system. The number of centroids used in quantization is optimized to minimize complexity for respective DSCM configurations while ensuring that the peak performance degradation after quantization is less than 0.01 dB. The quantization offers significant complexity reduction with minimal performance degradation across all sub-carrier symbol rates. Further, the complexity reduction achieved with quantization decreases with the sub-carriers symbol rates in the PM-DSCM-WDM system. Notably, the $(6\ \mathrm{GBd}\times 8)\times 5$ PM-DSCM-WDM system achieves a six-fold reduction in complexity compared to the simplistic $(48\ \mathrm{GBd}\times 1)\times 5$ WDM system, even without quantization. With quantization, this reduction is further enhanced to ten-fold, albeit with a slight compromise in performance gain.

Fig. 10 shows the average performance of WDM COI at peak transmit power and the corresponding complexities as functions of the number of adjacent sub-carriers considered for PB-NLC. Specifically, Fig. 10(a) and (b) represent the cases without and

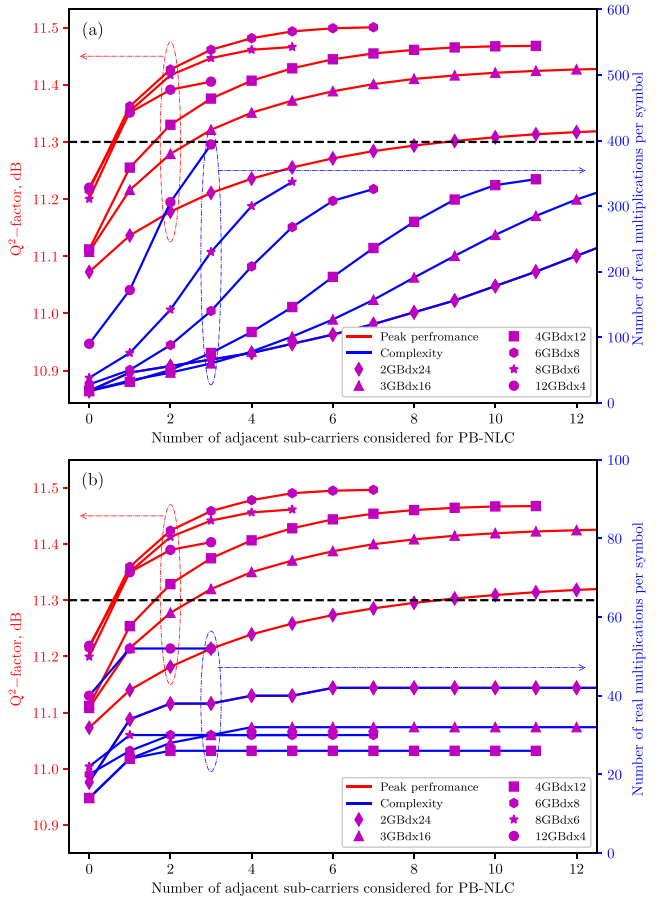

Fig. 10. Performance and computational complexity (a) without quantization and (b) with quantization of joint SRO and post-PB-NLC with different numbers of adjacent DSCM sub-carriers considered for PB-NLC.

with quantization, respectively. Different markers are utilized to represent distinct DSCM sub-carrier symbol rates. We exclude the 24 GBd and 48 GBd configurations in this comparison due to their high associated complexities. The plots are limited to a maximum of 12 adjacent sub-carriers. The quantization is optimized to minimize the complexity of PB-NLC, ensuring that the degradation in peak performance (considering all sub-carriers) after quantization is less than 0.01 dB. All performance curves in Fig. 10(a) without quantization and in Fig. 10(b) with quantization demonstrate rapid growth as the number of adjacent sub-carriers considered for the PB-NLC increases, eventually reaching a saturation point, regardless of the sub-carrier symbol rate.

The computational complexities in Fig. 10(a) without quantization increase continuously with the number of adjacent sub-carriers, but the gradient decreases as the number of adjacent sub-carriers considered for the PB-NLC grows. On the other hand, the computational complexities in Fig. 10(b) with quantization rapidly increase initially and then plateau. This observation can be explained as follows: The quantization process selects centroids to represent perturbation coefficients, without compromising the performance of PB-NLC. As the iXPM effects of far-away adjacent sub-carriers have less impact on the performance of PB-NLC, they do not increase the number of centroids as the number of adjacent sub-carriers increases. Therefore, the complexity of PB-NLC with quantization, which depends on the number of centroids representing the perturbation coefficients, resulting in a plateau in complexity as the number of adjacent sub-carriers increases. It is important to highlight that, considering symbol triplets from additional adjacent sub-carriers after the complexity curves plateau provides a further performance improvement. This improvement is achieved by utilizing the existing centroids with symbol triplets from additional adjacent sub-carriers. It is worth noting that considering more triplets corresponding to the same centroids does not require any additional real multiplications.

The numerical results in Fig. 10(a) and (b) facilitate the optimal system design based on specific performance or complexity requirements. For example, when a minimum performance threshold of 11.3 dB Q^2-factor (corresponding to a BER of about $3.8 \cdot 10^{-2}$) is mandated, the post-PB-NLC with quantization for PM-DSCM-WDM system with the lowest complexity is attained with the 4 GBd sub-carrier symbol rate, employing two adjacent sub-carriers for iXPM compensation (iXPM-2 with 4 GBd$\times$12). When PB-NLC is restricted to only use decisions from the SCOI, the best performance is attained with the 8 GBd$\times$6 DSCM configuration. Thus, joint SRO and PB-NLC provide an additional degree of freedom in selecting the number of adjacent sub-carriers for nonlinearity compensation to achieve a desired performance-complexity trade-off. Our analysis provides recommendations for selecting the symbol rate of DSCM and the number of adjacent sub-carriers to be considered for PB-NLC, aiming to achieve optimal system configurations in the practical implementation of joint SRO and PB-NLC within PM-DSCM-WDM systems to meet specific requirements.

E. Split PB-NLC for DSCM-WDM Systems

Finally, we address the integration of split PB-NLC derived in Section IV. Fig. 11 compares the average performances of the WDM COI for split PB-NLC and post-PB-NLC for the (6 GBd$\times$8) $\times$ 5 configuration. Curves for PB-NLC with iXPM-Full and iXPM-1 compensation are shown. We observe that split PB-NLC slightly outperforms post-PB-NLC. The gains are moderate as they are obtained by reducing the perturbation approximation errors and hard-decision decoding errors with pre-iXPM compensation. Most importantly, these gains are attained without additional computational cost, i.e., the total complexity at the transmitter and receiver is the same for split and post-PB-NLC.

The inset figure compares peak performances and corresponding computational complexities at the receiver, for the cases without and with quantization, for iXPM-Full compensation using post-PB-NLC and split PB-NLC. Before quantization, the complexity reduction at the receiver with split PB-NLC compared to post-PB-NLC is significant, at 44%. This trend remains consistent across various DSCM configurations, with systems with a larger number of sub-carriers experiencing more pronounced complexity reduction due to the dominant influence of iXPM effects. We apply two different quantization criteria

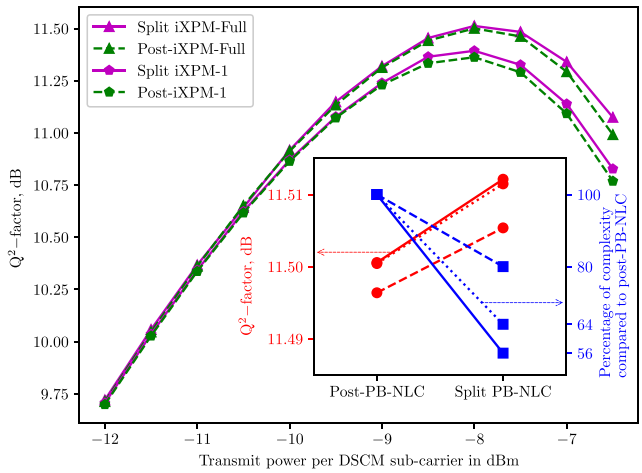

Fig. 11. Performance comparison of split PB-NLC and post-PB-NLC for the (6 GBd×8) × 5 configuration of the PM-DSCM-WDM system. Inset: Peak performances and corresponding computational complexities at the receiver without quantization (solid line) and with two quantization criteria (0.001 dB dotted line, 0.01 dB broken line) for iXPM-Full compensation with post-PB-NLC and split PB-NLC.

to both post-PB-NLC and split PB-NLC. The first quantization criterion minimizes complexity while ensuring that the peak performance degradation is less than 0.001 dB, whereas the second quantization criterion allows for a performance degradation of up to 0.01 dB. The first quantization criterion results in a 36% complexity reduction of split PB-NLC relative to post-PB-NLC at the receiver, whereas the second quantization criterion only yields a 20% complexity reduction for the same. These observations can be explained as follows: When a larger performance degradation is permitted, fewer quantized centroids are enough to achieve the desired performance threshold. Consequently, the number of common centroids representing the perturbation coefficients from the first half and second half of propagation increases. The split PB-NLC requires redundant multiplications for the common centroids. Therefore, the complexity reduction of split PB-NLC relative to post-PB-NLC at the receiver is contingent upon the chosen quantization. Specifically, the effectiveness of split PB-NLC compared to post-PB-NLC reduces as the acceptable performance degradation threshold increases.

Therefore, the proposed split PB-NLC offers a moderate gain and substantially reduced receiver complexity compared to post-PB-NLC. However, its effectiveness declines when performance degradation is permitted to achieve complexity reduction. It emerges as an ideal solution for complexity reduction in systems where performance is the crucial design criterion.

VI. Conclusion

Nonlinear effects present a significant challenge in enhancing the capacities of optical communication systems. Nonlinear mitigation and compensation techniques are utilized to counter these effects. However, their practical application is hindered by lower trade-offs between performance and complexity. Although combining nonlinear mitigation and compensation can enhance performance and complexity trade-offs, such combinations are frequently overlooked in the literature. Hence, a thorough investigation into the integration of nonlinear mitigation and compensation techniques is essential.

In this paper, we have proposed the joint fiber nonlinearity mitigation and compensation based on SRO and PB-NLC for pre-CDC transmission in the PM-DSCM-WDM system. We have shown that the joint approach affords an improved complexity-performance trade-off and flexibility in system design. For example, a 0.25 dB Q^2-factor gain with a tenfold reduction in computational complexity is achieved compared to the PM-WDM system with PB-NLC. Our simulation results have revealed that the optimum symbol rate of the PM-DSCM-WDM system is determined by which nonlinear effects (SPM, iXPM, and/or iFWM) are compensated and the extent (number of adjacent DSCM sub-carriers) to which these nonlinear effects are compensated by the nonlinearity compensation techniques. This highlights the potential of the SRO with respect to the nonlinearity compensation technique to achieve additional performance gain at no cost from joint nonlinearity mitigation and compensation. Finally, we have proposed a split PB-NLC that evenly distributes the (iXPM) PB-NLC between the transmitter and receiver by exploiting a unique property of iXPM for 50% pre-CDC transmission. Since split PB-NLC reduces the perturbation approximation and hard-decision decoding errors it also improves performance over post-PB-NLC.

Appendix A
Derivation of Post-PB-NLC in Conjunction With Pre-CDC

In this appendix, we obtain the pre-CDC transmit field for the WDM channel and the Manakov equation for the DSCM SCOI. We then apply a first-order perturbation approximation to the Manakov equation and use the transmit field as an initial condition to solve for the received field. Finally, we approximate the received signal in terms of transmit symbols and perturbation coefficients. This approximation is used to determine the PB-NLC in Sections III and IV.

A. Transmit Field

We consider the transmit field for a PM-DSCM-WDM channel as the sum of fields in the DSCM sub-carriers. Accordingly, the normalized initial field for a PM-DSCM-WDM channel before pre-CDC can be written as

$$\hat{\boldsymbol{u}}(z=0,t)=\sum_{\nu}\sum_{h}\boldsymbol{a}^{(\nu)}[h]g(z=0,t-hT_{\mathrm{s}})\times\exp(-\mathrm{j}\nu\Omega t), \tag{16}$$

where $\boldsymbol{a}^{(\nu)}[h]$ represents the transmit symbol of the ν^{th} DSCM sub-carrier at the h^{th} time slot, $g(z=0,t)$ is the basis pulse considered for both polarizations such that $\int_{-\infty}^{\infty} g(0,t-hT_{\mathrm{s}})g^{*}(0,t-h'T_{\mathrm{s}})dt=\delta_{h,h'}$, and T_{s} is the symbol duration. The center frequency of the DSCM SCOI is arbitrarily set to 0, and the center frequency of the ν^{th} adjacent DSCM sub-carrier is $\nu\Omega$, where Ω is the sub-carrier spacing. Applying

pre-CDC for the chromatic dispersion effects along a propagation length of L_c and using the frequency domain representation $G(z=0,\omega)=\int_{-\infty}^{\infty} g(z=0,t)\exp(\mathrm{j}\omega t)\mathrm{d}t$ [36], we obtain the pre-CDC transmit field as

$$\boldsymbol{u}(z=0,t)=\sum_{\nu}\sum_{h}\boldsymbol{a}^{(\nu)}[h]\int_{-\infty}^{\infty}G(z=0,\omega-\nu\Omega)\times\exp\left(j(\omega-\nu\Omega)hT_{\mathrm{s}}-\mathrm{j}\frac{\omega^2\beta_2 L_{\mathrm{c}}}{2}-\mathrm{j}\omega t\right)\frac{\mathrm{d}\omega}{2\pi}. \tag{17}$$

B. Manakov Equation for the DSCM SCOI

The Manakov-PMD (1) solves for the propagating field, $\boldsymbol{u}(z,t)$, at distance z and time t. We consider $\boldsymbol{u}(z,t)$ as the sum of fields from DSCM sub-carriers as

$$\boldsymbol{u}(z,t)=\sum_{\nu}\boldsymbol{u}^{(\nu)}(z,t). \tag{18}$$

As it is commonly done, we ignore the impact of PMD and noise on the nonlinearity [18], [21], and proceed with the simplified version of (1) as

$$\frac{\partial}{\partial z}\boldsymbol{u}(z,t)+\mathrm{j}\frac{\beta_2}{2}\frac{\partial^2}{\partial t^2}\boldsymbol{u}(z,t)=\mathrm{j}\frac{8}{9}\gamma|\boldsymbol{u}(z,t)|^2\boldsymbol{u}(z,t)f(z). \tag{19}$$

Applying the field in (18) to (19), we obtain the Manakov equation for the DSCM SCOI,

$$\frac{\partial}{\partial z}\boldsymbol{u}^{(0)}(z,t)+\mathrm{j}\frac{\beta_2}{2}\frac{\partial^2}{\partial t^2}\boldsymbol{u}^{(0)}(z,t)=\mathrm{j}\frac{8}{9}\gamma|\boldsymbol{u}^{(0)}(z,t)|^2\times\boldsymbol{u}^{(0)}(z,t)f(z)+\mathrm{j}\frac{8}{9}\gamma\sum_{\nu\neq 0}\left(|\boldsymbol{u}^{(\nu)}(z,t)|^2\boldsymbol{I}+\boldsymbol{u}^{(\nu)}(z,t)\boldsymbol{u}^{(\nu)\dagger}(z,t)\right)\boldsymbol{u}^{(0)}(z,t)f(z), \tag{20}$$

which incorporates the SPM and iXPM effects.

C. Received Field

The perturbation approach solves (20) by introducing the perturbation series in γ as

$$\boldsymbol{u}^{(0)}(z,t)=\sum_{k=0}^{\infty}\gamma^k\boldsymbol{u}_k^{(0)}(z,t). \tag{21}$$

Solving for order k yields

$$\frac{\partial}{\partial z}\boldsymbol{u}_k^{(0)}(z,t)+\mathrm{j}\frac{\beta_2}{2}\frac{\partial^2}{\partial t^2}\boldsymbol{u}_k^{(0)}(z,t)=\mathrm{j}\frac{8}{9}\times\sum_{p+q+r=k-1}\boldsymbol{u}_q^{(0)\dagger}(z,t)\boldsymbol{u}_p^{(0)}(z,t)\boldsymbol{u}_r^{(0)}(z,t)f(z)+\mathrm{j}\frac{8}{9}\sum_{\nu\neq 0}\sum_{p+q+r=k-1}\left(\boldsymbol{u}_q^{(\nu)\dagger}(z,t)\boldsymbol{u}_p^{(\nu)}(z,t)\boldsymbol{I}+\boldsymbol{u}_p^{(\nu)}(z,t)\boldsymbol{u}_q^{(\nu)\dagger}(z,t)\right)\boldsymbol{u}_r^{(0)}(z,t)f(z). \tag{22}$$

The first-order perturbation theory [20] considers the $k=0$ and $k=1$ terms from (21) and provides the approximate solution to the field of the SCOI at receiver distance $z=L$ as

$$\boldsymbol{u}^{(0)}(z=L,t)\approx\boldsymbol{u}_0^{(0)}(z=L,t)+\gamma\boldsymbol{u}_1^{(0)}(z=L,t). \tag{23}$$

Using the transmit field in (17) as the initial condition and solving (22) for $k=0$ and $k=1$ provides the zeroth- and first-order terms in (23) as

$$\boldsymbol{u}_0^{(0)}(z=L,t)=\sum_{h}\boldsymbol{a}^{(0)}[h]\int_{-\infty}^{\infty}G(z=0,\omega)\times\exp\left(\mathrm{j}\omega hT_{\mathrm{s}}+\mathrm{j}\frac{\omega^2\beta_2(L-L_{\mathrm{c}})}{2}-\mathrm{j}\omega t\right)\frac{\mathrm{d}\omega}{2\pi} \tag{24}$$

and

$$\boldsymbol{u}_1^{(0)}(z=L,t)=\int_{-\infty}^{\infty}\int_{0}^{L}\boldsymbol{F}(z,\omega)\times\exp\left(-\mathrm{j}\frac{\omega^2\beta_2(z-L)}{2}\right)\mathrm{d}z\exp(-\mathrm{j}\omega t)\frac{\mathrm{d}\omega}{2\pi}, \tag{25}$$

where

$$\boldsymbol{F}(z,\omega)=\mathrm{j}\frac{8}{9}\int_{-\infty}^{\infty}\left(\boldsymbol{u}_0^{(0)\dagger}(z,t)\boldsymbol{u}_0^{(0)}(z,t)\boldsymbol{u}_0^{(0)}(z,t)\times f(z)+\sum_{\nu\neq 0}\left(\boldsymbol{u}_0^{(\nu)\dagger}(z,t)\boldsymbol{u}_0^{(\nu)}(z,t)\boldsymbol{I}+\boldsymbol{u}_0^{(\nu)}(z,t)\boldsymbol{u}_0^{(\nu)\dagger}(z,t)\right)\boldsymbol{u}_0^{(0)}(z,t)f(z)\right)\exp(\mathrm{j}\omega t)\mathrm{d}t. \tag{26}$$

The zeroth-order field of the ν^{th} DSCM sub-carrier at distance z in (26), $\boldsymbol{u}_0^{(\nu)}(z,t)$, is

$$\boldsymbol{u}_0^{(\nu)}(z,t)=\exp\left(-\mathrm{j}\nu\Omega t+\mathrm{j}\frac{\nu^2\Omega^2\beta_2(z-L_{\mathrm{c}})}{2}\right)\times\sum_{h}\boldsymbol{a}^{(\nu)}[h]\int_{-\infty}^{\infty}G(z=0,\omega')\exp\left(\mathrm{j}\omega'\left(hT_{\mathrm{s}}+\nu\Omega\beta_2(z-L_{\mathrm{c}})\right)+\mathrm{j}\frac{\omega'^2\beta_2(z-L_{\mathrm{c}})}{2}-\mathrm{j}\omega' t\right)\frac{\mathrm{d}\omega'}{2\pi}, \tag{27}$$

where $\omega'=\omega-\nu\Omega$.

D. Received Signal

We consider the received field $\boldsymbol{u}^{(0)}(z=L,t)$ in (23) and apply post-CDC for the remaining CD effects from the propagation over the distance $L-L_{\mathrm{c}}$ and a matched filter proportional to $g^*(0,t-hT_{\mathrm{s}})$. After that, we consider the first-order perturbation value at $t=hT_{\mathrm{s}}$ because our nonlinearity compensation techniques are implemented at the symbol rate [20]. Based on nonlinear pulse collision [26], three pulse at time indices $(h+m)T_{\mathrm{s}}$, $(h+l)T_{\mathrm{s}}$ and $(h+n)T_{\mathrm{s}}$ generate a ghost pulse at hT_{s} when $l=m+n$. These operations provide the first-order

approximation of the received symbol for nonlinearity compensation as

$$\begin{aligned}\boldsymbol{b}^{(0)}[h] \approx \boldsymbol{a}^{(0)}[h] &+ \mathrm{j}\frac{8}{9}\gamma \sum_{m}\sum_{n} \boldsymbol{a}^{(0)^{\dagger}}[h+m+n] \\ &\times \boldsymbol{a}^{(0)}[h+m]\boldsymbol{a}^{(0)}[h+n]C_{m,n}^{(0)} \\ &+ \mathrm{j}\frac{8}{9}\gamma \sum_{\nu\neq 0}\sum_{m}\sum_{n}\Big(\boldsymbol{a}^{(\nu)^{\dagger}}[h+m+n]\boldsymbol{a}^{(\nu)}[h+m]\boldsymbol{I} \\ &+ \boldsymbol{a}^{(\nu)}[h+m]\boldsymbol{a}^{(\nu)^{\dagger}}[h+m+n]\Big)\boldsymbol{a}^{(0)}[h+n]C_{m,n}^{(\nu)}, \quad (28)\end{aligned}$$

where

$$\begin{aligned}C_{m,n}^{(\nu)} = \int_{-\infty}^{\infty}\int_{-\infty}^{\infty}\int_{-\infty}^{\infty} &\rho(\omega_1,\omega_2,\omega_3)\exp\left(\mathrm{j}\left(m\omega_1\right.\right. \\ &\left.\left. - (m+n)\omega_2 + n\omega_3\right)T_{\mathrm{s}}\right)\frac{\mathrm{d}^3\omega}{(2\pi)^3} \quad (29)\end{aligned}$$

is the perturbation coefficient,

$$\begin{aligned}\rho(\omega_1,\omega_2,\omega_3) = \tilde{G}(\omega_1,\omega_2,\omega_3)\int_0^L \exp\left(\mathrm{j}\Delta W\beta_2(z\right. \\ \left. - L_{\mathrm{c}})\right) f(z)\,\mathrm{d}z \quad (30)\end{aligned}$$

is the nonlinear kernel in the frequency domain [21],

$$\begin{aligned}\tilde{G}(\omega_1,\omega_2,\omega_3) = G(0,\omega_1)G^{*}(0,\omega_2)G(0,\omega_3) \\ \times G^{*}(0,\omega_1-\omega_2+\omega_3) \quad (31)\end{aligned}$$

is a quadruple product of the fundamental spectral pulse shape evaluated at four distinct angular frequencies and

$$\Delta W = (\omega_1-\omega_2)(\omega_2-\omega_3+\nu\Omega). \quad (32)$$

The value of ν is set to zero for the SPM perturbation coefficient ($C_{m,n}^{(0)}$) computation and adjusted according to the adjacent channel index ν for the iXPM perturbation coefficient ($C_{m,n}^{(\nu)}; \nu \neq 0$) computation.

Appendix B
Property of iXPM Used in Split PB-NLC

In this appendix, we explain the property of iXPM that is harnessed in the split PB-NLC. This property emerges from the interplay of dispersion, walk-off effect between the SCOI and the adjacent sub-carrier for the 50% pre-CDC transmission.

Fig. 12 shows the temporal evolution of three pulses transmitted at $t = (h-1)T$, $t = hT$, and $t = (h+1)T$ in two adjacent sub-carriers, with respect to a reference pulse transmitted at $t = hT$ in the SCOI, and at two locations in the fiber. The pulses propagate over time t_1. The adjacent sub-carrier frequencies are decreasing from adjacent sub-carrier 1, to the SCOI, to adjacent sub-carrier 2. Dispersion occurs as different frequencies within the pulses propagate at varying speeds, leading to temporal spreading at time $t = hT + t_1$. Walk-off arises because pulses with different sub-carrier frequencies travel at different speeds and thus different distances d_1, d_2, and d_3 during interval t_1, respectively, causing them to separate by distances $d_2 - d_1$ and $d_3 - d_2$ at time $t = hT + t_1$, respectively.

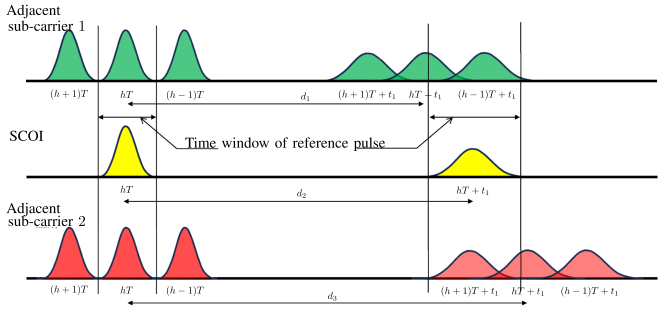

Fig. 12. Illustration of dispersion and walk-off, and pulse collision between adjacent sub-carriers for a transmission without pre-CDC. Left: location $z = 0$. Right: location $z = d_2$.

Let us consider adjacent sub-carrier 1 and the SCOI pulse propagation. The fastest frequency component in the sub-carrier 1 pulse transmitted at $t = (h+1)T$ lags behind and propagates more slowly than the slowest frequency component in the SCOI pulse transmitted at $t = hT$. Consequently, the sub-carrier 1 pulse transmitted at $t = (h+1)T$ avoids overlapping with the SCOI pulse transmitted at $t = hT$. For the same reason, sub-carrier 1 pulses transmitted prior at $t = hT, (h-1)T, (h-2)T, \ldots$ overlap with the SCOI pulse transmitted at $t = hT$. We observe an opposite dynamic when considering adjacent sub-carrier 2 and the SCOI. That is, the SCOI pulse transmitted at time $t = hT$ overlaps with the sub-carrier 2 pulses transmitted subsequently at $t = hT, (h+1)T, (h+2)T, \ldots$. Thus, iXPM effects result from the interaction between pulses in the SCOI and pulses with either negative or positive indices in adjacent sub-carriers, depending on the respective adjacent sub-carrier frequencies. Consequently, significant perturbation coefficients emerge only with negative or positive symbol indices linked to the involved pulses. This is shown in Fig. 2(c) for the iXPM perturbation coefficients corresponding to adjacent sub-carrier 2 for the scenario of no pre-CDC transmission. This attribute is also consistent with the XPM perturbation coefficients presented in [21, Fig. 1(d)].

The 50% pre-CDC transmission modifies the aforementioned attribute. Consider 50% pre-CDC transmission of a reference pulse propagating in the SCOI and two sequences of pulses propagating in adjacent sub-carriers with the frequencies considered in Fig. 12. Fig. 13 illustrates the temporal evolution of the pre-CDC pules at various points: at the transmitter side ($z = 0$), during the first half of the propagation ($0 < z < L/2$), at the halfway point ($z = L/2$), during the second half of the propagation ($L/2 < z < L$), and at the end of the propagation at the receiver ($z = L$). The pre-CDC broadens the pulses and adjusts the delays between adjacent sub-carriers at the transmitter to counter the dispersion and walk-off effects during the first half of the fiber propagation. The temporal widths corresponding to the pulse of interest in the SCOI at all locations are denoted by vertical demarcation lines. The solid (green and red) shaded pulses in adjacent sub-carriers share the same time index (before pre-CDC) as the reference pulse in the SCOI. Pulses at prior and subsequent time indices in adjacent sub-carriers are distinguished by different fill patterns.

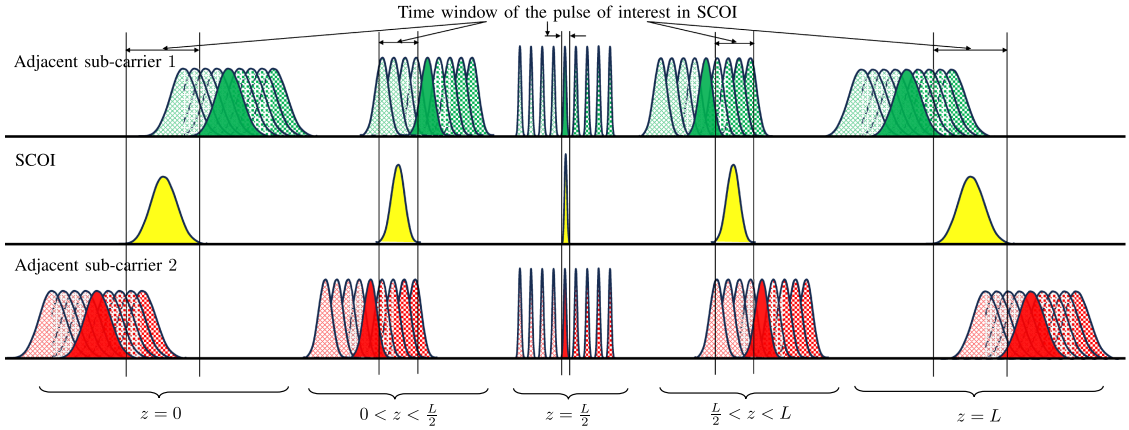

Fig. 13. Illustration of dispersion and walk-off, and pulse collision between adjacent sub-carriers for a transmission with pre-CDC.

Consider the propagation of pulses in the higher-frequency adjacent sub-carrier 1 with respect to the reference pulse in the SCOI. During the first half of the propagation, the pulse of interest in the SCOI overlaps with pulses in adjacent sub-carrier 1 of the same and subsequent indices. Dispersion and walk-off effects during this first half of the propagation completely reverse the pre-CDC effects for both the SCOI and the adjacent sub-carrier. Consequently, at $z = L/2$, the pulse of interest in the SCOI only overlaps with the pulse of the same index in adjacent sub-carrier 1. Subsequently, during the second half of propagation, the pulse of interest in the SCOI overlaps with pulses of the same and prior indices in adjacent sub-carrier 1. Therefore, distinct sets of pulses (those of the same and subsequent indices, and those of the same and prior indices concerning the pulse of interest) from adjacent sub-carrier 1 contribute to iXPM during the first and the second half of the propagation. Shifting our focus to adjacent sub-carrier 2, we observe the exact reverse dynamic in terms of symbol indices. Overall, the described pulse interactions result in the corresponding perturbation coefficients shown in Fig. 3(e) and (f). The split PB-NLC exploits this phenomenon to distribute computational complexity between the transmitter and receiver.

It is worth noting that finite-length and thus infinite-bandwidth pulses have been considered to illustrate the property. However, we use band-limited RRC pulses with a 0.1 roll-off factor in the computation of perturbation coefficients. These pulses cause a small temporal overlap between the prior and subsequent indices. Consequently, there is a small overlap between the perturbation coefficients for the first and second halves observed in Fig. 3(e) and (f).

REFERENCES

[1] P. J. Winzer, "Scaling optical fiber networks: Challenges and solutions," *Opt. Photon. News*, vol. 26, no. 3, pp. 28–35, Mar. 2015.

[2] C. A. Brackett, "Dense wavelength division multiplexing networks: Principles and applications," *IEEE J. Sel. Areas Commun.*, vol. 8, no. 6, pp. 948–964, Aug. 1990.

[3] L. Nelson, T. Nielsen, and H. Kogelnik, "Observation of PMD-induced coherent crosstalk in polarization-multiplexed transmission," *IEEE Photon. Technol. Lett.*, vol. 13, no. 7, pp. 738–740, Jul. 2001.

[4] E. Ip, A. P. T. Lau, D. J. Barros, and J. M. Kahn, "Coherent detection in optical fiber systems," *Opt. Exp.*, vol. 16, no. 2, pp. 753–791, Jan. 2008.

[5] E. Agrell et al., "Roadmap of optical communications," *J. Opt.*, vol. 18, no. 6, May 2016, Art. no. 063002.

[6] R. Olshansky, V. A. Lanzisera, and P. M. Hill, "Subcarrier multiplexed lightwave systems for broad-band distribution," *IEEE J. Lightw. Technol.*, vol. 7, no. 9, pp. 1329–1342, Sep. 1989.

[7] R. Hui, B. Zhu, R. Huang, C. T. Allen, K. R. Demarest, and D. Richards, "Subcarrier multiplexing for high-speed optical transmission," *IEEE J. Lightw. Technol.*, vol. 20, no. 3, pp. 417–427, Mar. 2002.

[8] G. P. Agrawal, *Nonlinear Fiber Optics (Sixth Edition)*. Cambridge, MA, USA:Academic Press, 2019.

[9] A. Mecozzi, C. B. Clausen, and M. Shtaif, "Analysis of intrachannel nonlinear effects in highly dispersed optical pulse transmission," *IEEE Photon. Technol. Lett.*, vol. 12, no. 4, pp. 392–394, Apr. 2000.

[10] S. Kumar and M. J. Deen, *Fiber Optic Communications: Fundamentals and Applications*. Hoboken, NJ, USA: Wiley, 2014.

[11] R. Dar and P. J. Winzer, "Nonlinear interference mitigation: Methods and potential gain," *IEEE J. Lightw. Technol.*, vol. 35, no. 4, pp. 903–930, Feb. 2017.

[12] P. Poggiolini et al., "Analytical and experimental results on system maximum reach increase through symbol rate optimization," *IEEE J. Lightw. Technol.*, vol. 34, no. 8, pp. 1872–1885, Apr. 2016.

[13] M. Qiu et al., "Digital subcarrier multiplexing for fiber nonlinearity mitigation in coherent optical communication systems," *Opt. Exp.*, vol. 22, no. 15, pp. 18770–18777, Jul. 2014.

[14] O. Geller, R. Dar, M. Feder, and M. Shtaif, "A shaping algorithm for mitigating inter-channel nonlinear phase-noise in nonlinear fiber systems," *IEEE J. Lightw. Technol.*, vol. 34, no. 16, pp. 3884–3889, Aug. 2016.

[15] Y. Gao et al., "Reducing the complexity of perturbation based nonlinearity pre-compensation using symmetric EDC and pulse shaping," *Opt. Exp.*, vol. 22, no. 2, pp. 1209–1219, Jan. 2014.

[16] E. Ip and J. M. Kahn, "Compensation of dispersion and nonlinear impairments using digital backpropagation," *IEEE J. Lightw. Technol.*, vol. 26, no. 20, pp. 3416–3425, Oct. 2008.

[17] V. Vgenopoulou, A. Amari, M. Song, E. Pincemin, I. Roudas, and Y. Jaouën, "Volterra-based nonlinear compensation in 400 Gb/s WDM multiband coherent optical OFDM systems," in *Proc. Asia Commun. Photon. Conf.*, 2014, pp. 1–3.

[18] O. S. Kumar, A. Amari, O. A. Dobre, and R. Venkatesan, "Enhanced regular perturbation-based nonlinearity compensation technique for optical transmission systems," *IEEE Photon. J.*, vol. 11, no. 4, Aug. 2019, Art. no. 7203612.

[19] A. Vannucci, P. Serena, and A. Bononi, "The RP method: A new tool for the iterative solution of the nonlinear Schrödinger equation," *IEEE J. Lightw. Technol.*, vol. 20, no. 7, pp. 1102–1112, Jul. 2002.

[20] Z. Tao, L. Dou, W. Yan, L. Li, T. Hoshida, and J. C. Rasmussen, "Multiplier-free intrachannel nonlinearity compensating algorithm operating at symbol rate," *IEEE J. Lightw. Technol.*, vol. 29, no. 17, pp. 2570–2576, Sep. 2011.

[21] F. Frey, L. Molle, R. Emmerich, C. Schubert, J. K. Fischer, and R. F. Fischer, "Single-step perturbation-based nonlinearity compensation of intra-and inter-subcarrier nonlinear interference," in *Proc. Eur. Conf. Opt. Commun.*, 2017, pp. 1–3.

[22] X. Liu, A. Chraplyvy, P. Winzer, R. Tkach, and S. Chandrasekhar, "Phase-conjugated twin waves for communication beyond the kerr nonlinearity limit," *Nature Photon.*, vol. 7, no. 7, pp. 560–568, Jul. 2013.

[23] R. Dar, M. Feder, A. Mecozzi, and M. Shtaif, "Properties of nonlinear noise in long, dispersion-uncompensated fiber links," *Opt. Exp.*, vol. 21, no. 22, pp. 25685–25699, Oct. 2013.

[24] O. Golani, M. Feder, and M. Shtaif, "NLIN mitigation using turbo equalization and an extended Kalman smoother," *IEEE J. Lightw. Technol.*, vol. 37, no. 9, pp. 1885–1892, May 2019.

[25] H. Bülow, "Experimental demonstration of optical signal detection using nonlinear fourier transform," *IEEE J. Lightw. Technol.*, vol. 33, no. 7, pp. 1433–1439, Apr. 2015.

[26] R. Dar, M. Feder, A. Mecozzi, and M. Shtaif, "Pulse collision picture of inter-channel nonlinear interference in fiber-optic communications," *IEEE J. Lightw. Technol.*, vol. 34, no. 2, pp. 593–607, Jan. 2016.

[27] F. Guiomar, A. Carena, G. Bosco, L. Bertignono, A. Nespola, and P. Poggiolini, "Nonlinear mitigation on subcarrier-multiplexed PM-16QAM optical systems," *Opt. Exp.*, vol. 25, no. 4, pp. 4298–4311, Feb. 2017.

[28] F. P. Guiomar, L. Bertignono, A. Nespola, P. Poggiolini, F. Forghieri, and A. Carena, "Combining probabilistic shaping and nonlinear mitigation: Potential gains and challenges," in *Proc. Opt. Fiber Commun. Conf.*,, Mar. 2018, pp. M3C–3.

[29] F. P. Guiomar, L. Bertignono, A. Nespola, and A. Carena, "Frequency-domain hybrid modulation formats for high bit-rate flexibility and nonlinear robustness," *IEEE J. Lightw. Technol.*, vol. 36, no. 20, pp. 4856–4870, Oct. 2018.

[30] A. Redyuk, E. Averyanov, O. Sidelnikov, M. Fedoruk, and S. Turitsyn, "Compensation of nonlinear impairments using inverse perturbation theory with reduced complexity," *IEEE J. Lightw. Technol.*, vol. 38, no. 6, pp. 1250–1257, Mar. 2020.

[31] T. Oyama et al., "Robust and efficient receiver-side compensation method for intra-channel nonlinear effects," in *Proc. Opt. Fiber Commun. Conf. Exhib.*, Mar. 2014, pp. 1–3.

[32] Y. Gao et al., "Joint pre-compensation and selective post-compensation for fiber nonlinearities," *IEEE Photon. Technol. Lett.*, vol. 26, no. 17, pp. 1746–1749, Sep. 2014.

[33] X. Liang, S. Kumar, J. Shao, M. Malekiha, and D. V. Plant, "Digital compensation of cross-phase modulation distortions using perturbation technique for dispersion-managed fiber-optic systems," *Opt. Exp.*, vol. 22, no. 17, pp. 20634–20645, Aug. 2014.

[34] D. Marcuse, C. Manyuk, and P. K. A. Wai, "Application of the Manakov-PMD equation to studies of signal propagation in optical fibers with randomly varying birefringence," *IEEE J. Lightw. Technol.*, vol. 15, no. 9, pp. 1735–1746, Sep. 1997.

[35] Z. Zheng et al., "Window-split structured frequency domain Kalman equalization scheme for large PMD and ultra-fast RSOP in an optical coherent PDM-QPSK system," *Opt. Exp.*, vol. 26, no. 6, pp. 7211–7226, Mar. 2018.

[36] R. Dar, M. Feder, A. Mecozzi, and M. Shtaif, "Inter-channel nonlinear interference noise in WDM systems: Modeling and mitigation," *IEEE J. Lightw. Technol.*, vol. 33, no. 5, pp. 1044–1053, Mar. 2015.

[37] Z. Tao, Y. Zhao, Y. Fan, L. Dou, T. Hoshida, and J. C. Rasmussen, "Analytical intrachannel nonlinear models to predict the nonlinear noise waveform," *IEEE J. Lightw. Technol.*, vol. 33, no. 10, pp. 2111–2119, May 2015.

[38] X. Liang and S. Kumar, "Multi-stage perturbation theory for compensating intra-channel nonlinear impairments in fiber-optic links," *Opt. Exp.*, vol. 22, no. 24, pp. 29733–29745, Dec. 2014.

[39] A. Amari, O. A. Dobre, R. Venkatesan, O. S. Kumar, P. Ciblat, and Y. Jaouën, "A survey on fiber nonlinearity compensation for 400 Gb/s and beyond optical communication systems," *IEEE Commun. Surveys Tuts.*, vol. 19, no. 4, pp. 3097–3113, Fourth quarter 2017.